ARTICLE TEMPLATE

Shape optimisation problem for stability of Navier-Stokes flow field

Yasuyuki Kiriyama[a], Eiji Katamine[b] and Hideyuki Azegami[a]

[a] Graduate School of Information Science, Nagoya University, A4-2 (780) Furo-cho, Chikusa-ku, Nagoya, Japan; [b] Department of Mechanical Engineering, National Institute of Technology, Gifu College, Gifu, Japan

ARTICLE HISTORY
Compiled July 20, 2018

ABSTRACT
This paper presents the numerical results of a shape optimisation problem with regard to delaying the transition of a Navier–Stokes flow field from laminar to turbulent by using the theory developed by Nakazawa and Azegami (2016). The theory was reviewed within the framework of functional analysis and updated with another expression of the shape derivative with respect to the objective function. A computer program was developed with the FreeFEM++. Numerical analyses were performed for two types of problems: a two-dimensional Poiseuille flow field with a sudden expansion, and a two-dimensional uniform flow field around an isolated body. From the first example, two local minimum points of symmetric and asymmetric flow fields were determined, and the asymmetric flow field was found to be more stable. With regard to the second example, we reached the local minimum point of an elliptical shape, and infrequently determined a solution converging to an elliptical shape with the bluff in the leeward direction. By comparison, the superiority of the elliptical shape was obvious.

KEYWORDS
Navier–Stokes flow; hydrodynamic stability; linear disturbance; shape optimisation; finite element method

1. Introduction

The flow field of a viscous fluid transitions from laminar to turbulent flow when the velocity increases. Situations wherein the laminar flow must be maintained exist not only in the design of fluid-related machinery, such as vehicles, but also in medical treatment related to blood flow. The main objective of this study was to demonstrate that we can obtain numerical solutions to shape the optimisation problem of the flow fields and delay the transition based on the theory presented by Nakazawa and Azegami (2016), who formulated the shape optimisation problem as described later. The state determination problems (with which solutions cost functions are defined) were defined with the stationary Navier–Stokes problem and an eigenvalue problem assuming a linear disturbance on the solution of the stationary Navier–Stokes problem. In the shape optimisation problem, the maximum value of the real parts of the eigenvalues is chosen as the objective cost function by using the solution of the eigenvalue problem because this value represents the rate at which the power of natural exponential function for

CONTACT Hideyuki Azegami. Email: azegami@i.nagoya-u.ac.jp

flow velocity and pressure increases with respect to time. This corresponds to the increasing rate of magnitude of the linear disturbance mode. The domain measure is used in a constraint cost function. The Fréchet derivatives of the cost functions with respect to an arbitrary domain variation, which we call the shape derivatives of the cost functions, are evaluated by using the shape derivative formulae of the domain and boundary integrals and the Lagrange multiplier method for the objective cost function. In a reshaping scheme, the H^1 gradient method is employed. This method will be explained later in more detail.

Various techniques to delay the transition have been reported in the literature. Strykowski and Sreenivasan (1990) investigated the phenomenon of vortex shedding behind a circular cylinder by appropriately placing a smaller cylinder in the near wake of the main cylinder. Numerical computations for the same situations were performed by Mittal and Raghuvanshi (2001). Hill (1992) used the regular and adjoint eigensolutions of the linearised incompressible Navier–Stokes equations to find the unstable mode based on the approach proposed by Jackson (1987) and Zebib (1987). Marquet, Sipp, and Jacquin (2008) investigated the sensitivity analysis of any global eigenvalue to the base-flow modifications induced by a steady force. Boujo and Gallaire (2014) demonstrated that the vortex shedding phenomenon can be confirmed by wall blowing/suction at the side of the cylinder. The stabilisation problem of flow using a passive control device in a sudden expansion channel has been investigated (Fani, Camarri, and Salvetti 2012). Moreover, active control by external forces in feedback systems has been applied to stabilise those flow fields (Belson et al. 2013; Camarri and Iollo 2010; Sipp et al. 2010). However, in these studies, the locations, sizes, and amplitudes were chosen as a target to control the instability of the phenomenon, and it was found that the geometrical shapes of the flow fields did not vary arbitrarily.

The shape optimisation theory of a flow field was developed by Pironneau (1973), who formulated the shape optimisation problem of an isolated body located in a uniform Stokes flow field to minimise drag power. Moreover, they derived the shape derivative with respect to the domain variation by an adjoint variable method based on the optimal control theory. Pironneau (1974, 1984) applied the theory to the Navier–Stokes equation. In subsequent work, Glowinski and Pironneau (1975) presented the numerical solutions for the minimum-drag profile of a two-dimensional body located within laminar flow by using a boundary-layer splicing method. Then, Sano and Sakai (1982) analysed the two-dimensional shape optimisation problems of an isolated body for Stokes flow fields by using the numerical procedure proposed by Pironneau, wherein the degrees of freedom of the finite element nodal points at the isolated body surface were chosen as the design variables, and an elliptical shape was obtained as the optimal shape. Additionally, Ganesh (1994) analysed a similar problem with a Reynolds number of 20 and obtained an ovoid, where the sharp end pointed to the upstream of the flow as the optimal shape. Huan and Modi (1994, 1996) analysed similar isolated body problems at a high Reynolds number. Ogawa and Kawahara (2003); Yagi and Kawahara (2005, 2007); Ishiyama and Kawahara (2008); Sakamoto and Kawahara (2011) also obtained the optimal shapes of an isolated body by choosing the coordinates of the finite element nodes at the boundary of an isolated body as the design variables, and used a discrete adjoint variable method. From a mathematical point of view, Bello et al. (1997) discussed the differentiability of the drag with respect to the variations of a Lipschitz domain in the Navier–Stokes flow.

For the aerodynamic design problems of velocity and pressure at the boundary of an isolated body, Jameson (1988) proposed the use of a continuous adjoint variable method to evaluate the shape derivatives of cost functions defined by the squared error

norms of velocity and pressure from specified values at the boundary of an isolated body. To overcome the irregularity of the shape derivatives, Jameson (1995) proposed using the smoothing equation of the shape derivative by applying a Laplacian operator at the boundary. The same idea has also been proposed by Mohammadi (1997) (Mohammadi and Pironneau 2001, p. 126 Eq. (5.1)). However, Katamine et al. (2005); Katamine, Nagatomo, and Azegami (2009) presented numerical results with regard to the minimisation problem of total dissipation energy in stationary viscous flow fields. In these studies, the H^1 gradient method was used for the shape optimisation problem. This method uses a Laplacian operator in the domain instead of the boundary, and the shape derivative as the Neumann boundary condition. This idea was first proposed as a traction method by Azegami (1994); Azegami and Wu (1996); Azegami and Takeuchi (2006), and has recently been named as the H^1 gradient method and used to systematisze a similar method for a topological optimisation problem with regard to the density type presented in Azegami, Kaizu, and Takeuchi (2011). The precise definition and basic properties of the H^1 gradient method for the shape optimisation problem have been presented by Azegami, Fukumoto, and Aoyama (2013); Azegami (2014, 2016).

As described earlier, in the investigation of flow field shape optimisation problems, the main focus has been on drag-power minimisation or on the squared error velocity and pressure norms. Studies focusing on the stability of the flow fields are rare. In such situations, the theory of delaying the transition, which has been presented by Nakazawa and Azegami (2016), should be investigated extensively. The objective of this study was to update the theory with another expression of the shape derivative, with respect to the objective function used in Nakazawa and Azegami (2016), and present numerical results with regard to two types of problems: a two-dimensional Poiseuille flow field with a sudden expansion, and a two-dimensional uniform flow field around an isolated body.

In this study, we used the notation of $W^{s,p}(D;\mathbb{R})$ to represent the Sobolev space for the set of functions defined in D, having value of $\mathbb{R}$ ($\mathbb{R}$ denotes the set of real numbers) and being $s \in [0,\infty]$ times differentiable and $p \in [1,\infty]$th order Lebesgue integrable. Moreover, $W^{0,p}\left(\Omega_0;\mathbb{R}^d\right)$ and $W^{s,2}\left(\Omega_0;\mathbb{R}^d\right)$ are denoted by $L^p\left(\Omega_0;\mathbb{R}^d\right)$ and $H^s\left(\Omega_0;\mathbb{R}^d\right)$, respectively. With respect to the reflexive Sobolev space X, we denote its dual space by X' and the dual product of $(x,y) \in X \times X'$ by $\langle x,y\rangle$. Specifically, $f'(\boldsymbol{x})[\boldsymbol{y}]$ represents the Fréchet derivative $\langle f'(\boldsymbol{x}),\boldsymbol{y}\rangle$ of $f : X \to \mathbb{R}$ at $\boldsymbol{x} \in X$ with respect to an arbitrary variation $\boldsymbol{y} \in X$. Additionally, $f_{\boldsymbol{x}}(\boldsymbol{x},\boldsymbol{y})[\boldsymbol{z}]$ represents the Fréchet partial derivative. The notation $\forall$ corresponds to 'for all', and $\boldsymbol{A}\cdot\boldsymbol{B}$ represents the scalar product $\sum_{(i,j)\in\{1,\dots,m\}^2} a_{ij}b_{ij}$ with respect to $\boldsymbol{A} = (a_{ij})_{ij}$, $\boldsymbol{B} = (b_{ij})_{ij} \in \mathbb{R}^{m\times m}$.

2. Initial domain and set of domain variations

Figure 1 shows the domain variation from the initial domain $\Omega_0 \subset \mathbb{R}^d$ ($d \in \{2,3\}$) of the flow field. We assume that Ω_0 has a $\partial\Omega_0$ Lipschitz boundary, $\Gamma_{\mathrm{D}0} \subset \partial\Omega_0$ is a Dirichlet boundary for which the flow velocity is given, and $\Gamma_{\mathrm{N}0} = \partial\Omega_0 \setminus \bar{\Gamma}_{\mathrm{D}0}$ ($\bar{(\cdot)}$ denotes a closure) is a Neumann boundary for which the condition of the flow velocity and pressure gradient is given. In this study, the domain after Ω_0 has moved was formed by a continuous one-to-one onto mapping $\boldsymbol{i}+\boldsymbol{\phi} : \mathbb{R}^d \to \mathbb{R}^d$ as $(\boldsymbol{i}+\boldsymbol{\phi})(\Omega_0) = \{(\boldsymbol{i}+\boldsymbol{\phi})(\boldsymbol{x}) \mid \boldsymbol{x} \in \Omega_0\}$ using $\boldsymbol{i}$ as the identity mapping and denoted as $\Omega(\boldsymbol{\phi})$. Similarly, with respect to the initial domain or boundary $(\cdot)_0$, $(\cdot)(\boldsymbol{\phi})$ rep-

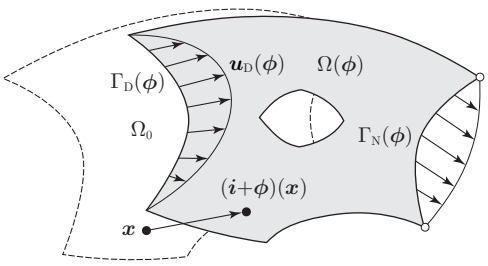

Figure 1. Initial domain $\Omega_0 \subset \mathbb{R}^d$ and domain variation (displacement) $\boldsymbol{\phi}$ for Navier–Stokes flow field.

resents $\{(\boldsymbol{i}+\boldsymbol{\phi})(\boldsymbol{x}) \mid \boldsymbol{x} \in (\cdot)_0\}$. Hence, $\boldsymbol{\phi}$ represents the displacement in the domain variation. In the shape optimisation problem, we set $\boldsymbol{\phi}$ as the design variable.

The function spaces for $\boldsymbol{\phi}$ are defined as follows. Because we will consider the gradient method in a function space later, the function space containing $\boldsymbol{\phi}$ must be a Hilbert space. Hence, we set

$$X = \left\{ \boldsymbol{\phi} \in H^1\left(\mathbb{R}^d; \mathbb{R}^d\right) \;\middle|\; \boldsymbol{\phi} = \boldsymbol{0}_{\mathbb{R}^d} \text{ on } \bar{\Omega}_{\mathrm{C}0} \right\}, \tag{1}$$

as the linear space for $\boldsymbol{\phi}$, where $\bar{\Omega}_{\mathrm{C}0} \subset \bar{\Omega}_0$ represents a boundary or domain closure, where the domain variation is constrained owing to the design requirements. When $\boldsymbol{\phi}$ is an element of X, there is no guarantee that $\Omega(\boldsymbol{\phi})$ will be a Lipschitz domain. To ensure the possibility of becoming a Lipschitz domain, $\boldsymbol{\phi}$ has to be an element of $W^{1,\infty}\left(\mathbb{R}^d; \mathbb{R}^d\right)$. Thus, the admissible set for $\boldsymbol{\phi}$ must be set as

$$\mathcal{D} = \left\{ \boldsymbol{\phi} \in X \cap W^{1,\infty}\left(\mathbb{R}^d; \mathbb{R}^d\right) \;\middle|\; \boldsymbol{\phi} \text{ is bijection, } \partial\Omega(\boldsymbol{\phi}) \text{ is Lipschitz} \right\}. \tag{2}$$

3. State determination problems

If a $\boldsymbol{\phi} \in \mathcal{D}$ is given, a stationary Navier–Stokes problem and an eigenvalue problem assuming a linear disturbance to the solution of the stationary Navier–Stokes problem can be defined as described later with respect to $\Omega(\boldsymbol{\phi})$.

3.1. *Navier–Stokes problem*

With respect to $\boldsymbol{\phi} \in \mathcal{D}$, we assume that $\boldsymbol{u}_{\mathrm{D}} : \mathbb{R}^d \to \mathbb{R}^d$ satisfying $\boldsymbol{\nabla} \cdot \boldsymbol{u}_{\mathrm{D}} = 0$ is given. Let $\boldsymbol{u}$ denote flow velocity, and its function spaces be defined as

$$\begin{aligned}
&U = \left\{ \boldsymbol{u} \in H^1\left(\Omega(\boldsymbol{\phi}); \mathbb{R}^d\right) \;\middle|\; \boldsymbol{u} = \boldsymbol{0}_{\mathbb{R}^d} \text{ on } \Gamma_{\mathrm{D}}(\boldsymbol{\phi}) \right\}, \\
&U(\boldsymbol{u}_{\mathrm{D}}) = \left\{ \boldsymbol{u} \in H^1\left(\Omega(\boldsymbol{\phi}); \mathbb{R}^d\right) \;\middle|\; \boldsymbol{u} = \boldsymbol{u}_{\mathrm{D}} \text{ on } \Gamma_{\mathrm{D}}(\boldsymbol{\phi}) \right\}, \\
&\mathcal{S} = U \cap W^{1,\infty}\left(\Omega(\boldsymbol{\phi}); \mathbb{R}^d\right), \quad \mathcal{S}(\boldsymbol{u}_{\mathrm{D}}) = U(\boldsymbol{u}_{\mathrm{D}}) \cap W^{1,\infty}\left(\Omega(\boldsymbol{\phi}); \mathbb{R}^d\right).
\end{aligned}$$

The function spaces for pressure p are set as

$$P = L^2(\Omega(\boldsymbol{\phi}); \mathbb{R}), \quad \mathcal{Q} = P \cap L^\infty(\Omega(\boldsymbol{\phi}); \mathbb{R}).$$

Moreover, μ and ρ are the positive constants representing the viscosity and density coefficients. $(\boldsymbol{\nu}\cdot\boldsymbol{\nabla})\,\boldsymbol{u} = \left(\boldsymbol{\nabla}\boldsymbol{u}^{\mathrm{T}}\right)^{\mathrm{T}}\boldsymbol{\nu}$ can be written as $\partial_{\nu}\boldsymbol{u}$. In this case, we define a stationary Navier–Stokes problem as a state determination problem in the flow field shape optimisation problem, as described later.

Problem 3.1 (Stationary Navier–Stokes problem)**.** *With respect to $\boldsymbol{\phi}\in\mathcal{D}$, and assuming that $\Omega(\boldsymbol{\phi})$ and $\boldsymbol{u}_{\mathrm{D}}$ are given with appropriate regularity, find $(\boldsymbol{u},p)\in\mathcal{S}\times\mathcal{Q}$ such that*

$$\rho(\boldsymbol{u}\cdot\boldsymbol{\nabla})\,\boldsymbol{u}^{\mathrm{T}} - \boldsymbol{\nabla}^{\mathrm{T}}\left(\mu\boldsymbol{\nabla}\boldsymbol{u}^{\mathrm{T}}\right) + \boldsymbol{\nabla}^{\mathrm{T}}p = \boldsymbol{b}^{\mathrm{T}} \quad \textit{in } \Omega(\boldsymbol{\phi}), \tag{3}$$

$$\boldsymbol{\nabla}\cdot\boldsymbol{u} = 0 \quad \textit{in } \Omega(\boldsymbol{\phi}), \tag{4}$$

$$\boldsymbol{u} = \boldsymbol{u}_{\mathrm{D}} \quad \textit{on } \Gamma_{\mathrm{D}}(\boldsymbol{\phi}), \tag{5}$$

$$\mu\partial_{\nu}\boldsymbol{u} - p\boldsymbol{\nu} = \boldsymbol{0}_{\mathbb{R}^d} \quad \textit{on } \Gamma_{\mathrm{N}}(\boldsymbol{\phi}). \tag{6}$$

In the case of unsteady flow, with respect to $(\boldsymbol{u},p):\mathbb{R}\times\Omega(\boldsymbol{\phi})\to\mathbb{R}^{d+1}$, (3) and (4) are rewritten as

$$\rho\boldsymbol{u}_t^{\mathrm{T}} + \rho(\boldsymbol{u}\cdot\boldsymbol{\nabla})\,\boldsymbol{u}^{\mathrm{T}} - \boldsymbol{\nabla}^{\mathrm{T}}\left(\mu\boldsymbol{\nabla}\boldsymbol{u}^{\mathrm{T}}\right) + \boldsymbol{\nabla}^{\mathrm{T}}p = \boldsymbol{b}^{\mathrm{T}} \quad \text{in } \mathbb{R}\times\Omega(\boldsymbol{\phi}), \tag{7}$$

$$\boldsymbol{\nabla}\cdot\boldsymbol{u} = 0 \quad \text{in } \mathbb{R}\times\Omega(\boldsymbol{\phi}), \tag{8}$$

where $\boldsymbol{u}_t$ denotes the partial derivative with respect to time $t\in\mathbb{R}$.

3.2. *Linear disturbance eigenvalue problem*

By using the $(\boldsymbol{u},p)$ solution of Problem 3.1, an eigenvalue problem that assumes a linear disturbance in the solution can be defined as described below. Here, we represent the solution of Problem 3.1 as $(\boldsymbol{u}(0,\boldsymbol{x}),p(0,\boldsymbol{x}))$ with respect to $\boldsymbol{x}\in\Omega(\boldsymbol{\phi})$, and assume the following form:

$$\boldsymbol{u}(\tau,\boldsymbol{x}) = \boldsymbol{u}(0,\boldsymbol{x}) + \bar{\boldsymbol{u}}(\tau,\boldsymbol{x}) \quad \text{in } [0,\infty)\times\Omega(\boldsymbol{\phi}), \tag{9}$$

$$p(\tau,\boldsymbol{x}) = p(0,\boldsymbol{x}) + \bar{p}(\tau,\boldsymbol{x}) \quad \text{in } [0,\infty)\times\Omega(\boldsymbol{\phi}), \tag{10}$$

where $(\bar{\boldsymbol{u}}(\tau,\boldsymbol{x}),\bar{p}(\tau,\boldsymbol{x}))$ represents the disturbance component. By substituting $(\boldsymbol{u}(\tau,\boldsymbol{x}),p(\tau,\boldsymbol{x}))$ of (9) and (10) into (7) and (8), considering that $(\boldsymbol{u}(0,\boldsymbol{x}),p(0,\boldsymbol{x}))$ is the solution of Problem 3.1, and neglecting terms higher than the second order of $(\bar{\boldsymbol{u}}(\tau,\boldsymbol{x}),\bar{p}(\tau,\boldsymbol{x}))$, (7) and (8) become

$$\begin{aligned}&\rho\bar{\boldsymbol{u}}_{\tau}^{\mathrm{T}} + \rho(\boldsymbol{u}\cdot\boldsymbol{\nabla})\,\bar{\boldsymbol{u}}^{\mathrm{T}} + \rho(\bar{\boldsymbol{u}}\cdot\boldsymbol{\nabla})\,\boldsymbol{u}^{\mathrm{T}}\\ &\qquad -\boldsymbol{\nabla}^{\mathrm{T}}\left(\mu\boldsymbol{\nabla}\bar{\boldsymbol{u}}^{\mathrm{T}}\right) + \boldsymbol{\nabla}^{\mathrm{T}}\bar{p} = \boldsymbol{0}_{\mathbb{R}^d}^{\mathrm{T}} \quad \text{in } [0,\infty)\times\Omega(\boldsymbol{\phi}),\end{aligned} \tag{11}$$

$$\boldsymbol{\nabla}\cdot\bar{\boldsymbol{u}} = 0 \quad \text{in } [0,\infty)\times\Omega(\boldsymbol{\phi}), \tag{12}$$

where $(\boldsymbol{u},p)$ and $(\bar{\boldsymbol{u}},\bar{p})$ represent $(\boldsymbol{u}(0,\boldsymbol{x}),p(0,\boldsymbol{x}))$ and $(\bar{\boldsymbol{u}}(\tau,\boldsymbol{x}),\bar{p}(\tau,\boldsymbol{x}))$, respectively. Moreover, we assume that $(\bar{\boldsymbol{u}}(\tau,\boldsymbol{x}),\bar{p}(\tau,\boldsymbol{x}))$ are separable with respect to the functions of time and space as

$$\bar{\boldsymbol{u}}(\tau,\boldsymbol{x}) = \mathrm{e}^{s\tau}\hat{\boldsymbol{u}}(\boldsymbol{x}) + \mathrm{e}^{s^{\mathrm{c}}\tau}\hat{\boldsymbol{u}}^{\mathrm{c}}(\boldsymbol{x}) = 2\mathrm{Real}\left[\mathrm{e}^{s\tau}\hat{\boldsymbol{u}}(\boldsymbol{x})\right] \quad \text{in } [0,\infty)\times\Omega(\boldsymbol{\phi}), \tag{13}$$

$$\bar{p}(\tau,\boldsymbol{x}) = 2\mathrm{Real}\left[\mathrm{e}^{s\tau}\hat{p}(\boldsymbol{x})\right] \quad \text{in } [0,\infty)\times\Omega(\boldsymbol{\phi}), \tag{14}$$

where $s \in \mathbb{C}$ ($\mathbb{C}$ denotes the set of complex numbers) and $(\hat{\boldsymbol{u}}(\boldsymbol{x}), \hat{p}(\boldsymbol{x})) \in \hat{\mathcal{S}} \times \hat{\mathcal{Q}} \subset \hat{U} \times \hat{P}$ are defined as

$$\begin{aligned}
\hat{U} &= \left\{ \hat{\boldsymbol{u}} \in H^1\left(\Omega(\boldsymbol{\phi}); \mathbb{C}^d\right) \mid \hat{\boldsymbol{u}} = \boldsymbol{0}_{\mathbb{R}^d} \text{ on } \Gamma_{\mathrm{D}}(\boldsymbol{\phi}) \right\}, \\
\hat{\mathcal{S}} &= \hat{U} \cap W^{1,\infty}\left(\Omega(\boldsymbol{\phi}); \mathbb{C}^d\right), \\
\hat{P} &= \hat{q} \in L^2(\Omega(\boldsymbol{\phi}); \mathbb{C}), \quad \hat{\mathcal{Q}} = \hat{P} \cap L^\infty(\Omega(\boldsymbol{\phi}); \mathbb{C}).
\end{aligned}$$

Here, by substituting (13) and (14) into (11) and (12), and considering the boundary conditions, the following eigenvalue problem with respect to the eigenvalue s and eigenfunction $(\hat{\boldsymbol{u}}(\boldsymbol{x}), \hat{p}(\boldsymbol{x}))$ can be obtained. Thereby, we can write $(\boldsymbol{u}(0, \boldsymbol{x}), p(0, \boldsymbol{x}))$ and $(\hat{\boldsymbol{u}}(\boldsymbol{x}), \hat{p}(\boldsymbol{x}))$ as $(\boldsymbol{u}, p)$ and $(\hat{\boldsymbol{u}}, \hat{p})$, respectively.

Problem 3.2 (Linear disturbance eigenvalue problem)**.** *When the solution $(\boldsymbol{u}, p)$ of Problem 3.1 with respect to $\boldsymbol{\phi} \in \mathcal{D}$ is obtained, find $(s_r, \hat{\boldsymbol{u}}_r, \hat{p}_r) \in \mathbb{C} \times \hat{\mathcal{S}} \times \hat{\mathcal{Q}}$ for $r \in \mathbb{N}$ ($\mathbb{N}$ denotes the set of natural numbers) satisfying*

$$\begin{aligned}
\rho s_r \hat{\boldsymbol{u}}_r^{\mathrm{T}} + \rho(\boldsymbol{u} \cdot \boldsymbol{\nabla}) \hat{\boldsymbol{u}}_r^{\mathrm{T}} + \rho(\hat{\boldsymbol{u}}_r \cdot \boldsymbol{\nabla}) \boldsymbol{u}^{\mathrm{T}} - \boldsymbol{\nabla}^{\mathrm{T}}\left(\mu \boldsymbol{\nabla} \hat{\boldsymbol{u}}_r^{\mathrm{T}}\right) + \boldsymbol{\nabla}^{\mathrm{T}} \hat{p}_r &= \boldsymbol{0}_{\mathbb{C}^d}^{\mathrm{T}} \quad \textit{in } \Omega(\boldsymbol{\phi}), \\
\boldsymbol{\nabla} \cdot \hat{\boldsymbol{u}}_r &= 0 \quad \textit{in } \Omega(\boldsymbol{\phi}), \\
\hat{\boldsymbol{u}}_r &= \boldsymbol{0}_{\mathbb{C}^d} \quad \textit{on } \Gamma_{\mathrm{D}}(\boldsymbol{\phi}), \\
\mu \partial_\nu \hat{\boldsymbol{u}}_r - \hat{p}_r \boldsymbol{\nu} &= \boldsymbol{0}_{\mathbb{C}^d} \quad \textit{on } \Gamma_{\mathrm{N}}(\boldsymbol{\phi}).
\end{aligned}$$

Problem 3.2 is a complex eigenvalue problem. By focusing on the stability of the flow field, it can be considered that an unstable phenomenon occurs when the maximum value of the eigenvalues' real parts becomes positive because this value represents the rate by which the power of natural exponential function for flow velocity and pressure increases with respect to time as defined in (13) and (14). Moreover, the magnitude of eigenfunction $(\hat{\boldsymbol{u}}_r, \hat{p}_r)$ in Problem 3.2 is indefinite. In this study, we used the following normalisation condition:

$$\int_{\Omega(\boldsymbol{\phi})} \rho \hat{\boldsymbol{u}}_r \cdot \hat{\boldsymbol{u}}_r^{\mathrm{c}} \, \mathrm{d}x = 1, \tag{15}$$

where $(\cdot)^{\mathrm{c}}$ denotes the complex conjugate.

4. Shape optimisation problem

By using the solutions of Problems 3.1 and 3.2, a shape optimisation problem can be defined as described later. In this study, we set the mode orders $r \in \mathbb{N}$ of the eigenvalues in descending order with respect to the real part. Based on the ordering, we set

$$f_0(s_1) = s_1 + s_1^{\mathrm{c}} = 2\mathrm{Real}[s_1] \tag{16}$$

as an objective cost function. Moreover, the following constraint cost function was used to restrict the domain measure of the flow field:

$$f_1(\boldsymbol{\phi}) = \int_{\Omega(\boldsymbol{\phi})} \mathrm{d}x - c_1, \tag{17}$$

where c_1 is a positive constant such that there exists a $\boldsymbol{\phi} \in \mathcal{D}$ satisfying $f_1(\boldsymbol{\phi}) \leq 0$.

Problem 4.1 (Minimization of disturbance eigenvalue's maximum real part)**.** *Find* $\Omega(\boldsymbol{\phi})$ *such that*

$$\min_{(\boldsymbol{\phi},\boldsymbol{u},p,s_1,\hat{\boldsymbol{u}}_1,\hat{p}_1)\in\mathcal{D}\times\mathcal{S}(\boldsymbol{u}_\mathrm{D})\times\mathcal{Q}\times\mathbb{C}\times\hat{\mathcal{S}}\times\hat{\mathcal{Q}}} \left\{ f_0(s_1) \;\middle|\; f_1(\boldsymbol{\phi}) \leq 0,\ \textit{Problems 3.1 and 3.2} \right\}.$$

5. Shape derivatives of cost functions

To use a gradient method for solving Problem 4.1, the Fréchet derivatives of the cost functions with respect to the arbitrary variation of the design variable are required. In this study, we adopted Definition .2, which is provided in the Appendix, with respect to the shape derivative of a functional, and sought the shape derivatives of $f_0(s_1)$ and $f_1(\boldsymbol{\phi})$ with respect to the arbitrary variation $\boldsymbol{\varphi} \in \mathcal{D}$ of the design variable $\boldsymbol{\phi} \in \mathcal{D}$.

5.1. *Shape derivative of* f_0

To count the state determination problems as equality constraints, we used the Lagrange multiplier method. The Lagrange function of $f_0(s_1)$ is defined as

$$\begin{aligned}
&\mathscr{L}_0(\boldsymbol{\phi}, \boldsymbol{u}, p, \boldsymbol{v}_0, q_0, s_1, \hat{\boldsymbol{u}}_1, \hat{p}_1, \hat{\boldsymbol{v}}_0^\mathrm{c}, \hat{q}_0^\mathrm{c}) \\
&\quad = f_0(s_1) - \mathscr{L}_\mathrm{S}(\boldsymbol{\phi}, \boldsymbol{u}, p, \boldsymbol{v}_0, q_0) - \hat{\mathscr{L}}_\mathrm{S}(\boldsymbol{\phi}, s_1, \boldsymbol{u}, \hat{\boldsymbol{u}}_1, \hat{p}_1, \hat{\boldsymbol{v}}_0^\mathrm{c}, \hat{q}_0^\mathrm{c}),
\end{aligned}$$

where $\mathscr{L}_\mathrm{S}(\boldsymbol{\phi}, \boldsymbol{u}, p, \boldsymbol{v}_0, q_0)$ and $\hat{\mathscr{L}}_\mathrm{S}(\boldsymbol{\phi}, s_1, \boldsymbol{u}, \hat{\boldsymbol{u}}_1, \hat{p}_1, \hat{\boldsymbol{v}}_0^\mathrm{c}, \hat{q}_0^\mathrm{c})$ are the Lagrange functions with respect to Problems 3.1 and 3.2, respectively, and defined as

$$\begin{aligned}
&\mathscr{L}_\mathrm{S}(\boldsymbol{\phi}, \boldsymbol{u}, p, \boldsymbol{v}_0, q_0) \\
&\quad = \int_{\Omega(\boldsymbol{\phi})} \left\{ -\rho\left((\boldsymbol{u}\cdot\boldsymbol{\nabla})\boldsymbol{u}\right)\cdot\boldsymbol{v}_0 - \mu\left(\boldsymbol{\nabla}\boldsymbol{u}^\mathrm{T}\right)\cdot\left(\boldsymbol{\nabla}\boldsymbol{v}_0^\mathrm{T}\right) + p\boldsymbol{\nabla}\cdot\boldsymbol{v}_0 + q_0\boldsymbol{\nabla}\cdot\boldsymbol{u} + \boldsymbol{b}\cdot\boldsymbol{v}_0 \right\}\mathrm{d}x \\
&\qquad + \int_{\partial\Omega(\boldsymbol{\phi})} \left\{ (\boldsymbol{u}-\boldsymbol{u}_\mathrm{D})\cdot(\mu\partial_\nu\boldsymbol{v}_0 - q_0\boldsymbol{\nu}) + \boldsymbol{v}_0\cdot(\mu\partial_\nu\boldsymbol{u} - p\boldsymbol{\nu}) \right\}\mathrm{d}\gamma. \\
&\hat{\mathscr{L}}_\mathrm{S}(\boldsymbol{\phi}, s_1, \boldsymbol{u}, \hat{\boldsymbol{u}}_1, \hat{p}_1, \hat{\boldsymbol{v}}_0^\mathrm{c}, \hat{q}_0^\mathrm{c}) \\
&\quad = 2\mathrm{Real}\Bigg[\int_{\Omega(\boldsymbol{\phi})} \Big[-\rho s_1 \hat{\boldsymbol{u}}_1\cdot\hat{\boldsymbol{v}}_0^\mathrm{c} - \rho\left\{(\boldsymbol{u}\cdot\boldsymbol{\nabla})\hat{\boldsymbol{u}}_1\right\}\cdot\hat{\boldsymbol{v}}_0^\mathrm{c} - \rho\left\{(\hat{\boldsymbol{u}}_1\cdot\boldsymbol{\nabla})\boldsymbol{u}\right\}\cdot\hat{\boldsymbol{v}}_0^\mathrm{c} \\
&\qquad - \mu\left(\boldsymbol{\nabla}\hat{\boldsymbol{u}}_1^\mathrm{T}\right)\cdot\left(\boldsymbol{\nabla}\hat{\boldsymbol{v}}_0^{\mathrm{c}\mathrm{T}}\right) + \hat{p}_1\boldsymbol{\nabla}\cdot\hat{\boldsymbol{v}}_0^\mathrm{c} + \hat{q}_0^\mathrm{c}\boldsymbol{\nabla}\cdot\hat{\boldsymbol{u}}_1 \Big]\mathrm{d}x \\
&\qquad + \int_{\Gamma_\mathrm{D}(\boldsymbol{\phi})} \left\{ \hat{\boldsymbol{u}}_1\cdot(\mu\partial_\nu\hat{\boldsymbol{v}}_0^\mathrm{c} - \hat{q}_0^\mathrm{c}\boldsymbol{\nu}) + \hat{\boldsymbol{v}}_0^\mathrm{c}\cdot(\mu\partial_\nu\hat{\boldsymbol{u}}_1 - \hat{p}_1\boldsymbol{\nu}) \right\}\mathrm{d}\gamma \Bigg].
\end{aligned}$$

Here, $(\boldsymbol{v}_0, q_0) \in U \times P$ and $(\hat{\boldsymbol{v}}_0, \hat{q}_0) \in \hat{U} \times \hat{P}$ are the Lagrange multipliers with respect to Problems 3.1 and 3.2, respectively, which are provided for f_0.

Here, we assume that $\boldsymbol{u}_{\mathrm{D}}$ moves with the domain variation $(\boldsymbol{u}'_{\mathrm{D}}(\boldsymbol{\phi})[\boldsymbol{\varphi}] = \boldsymbol{0}_{\mathbb{R}^d}$ by using Definition .1) to take the shape derivative of $\mathscr{L}_0(\boldsymbol{\phi}, \boldsymbol{u}, p, \boldsymbol{v}_0, q_0, s_1, \hat{\boldsymbol{u}}_1, \hat{p}_1, \hat{\boldsymbol{v}}_0^{\mathrm{c}}, \hat{q}_0^{\mathrm{c}})$ using Propositions .3 and .4, and obtain the following notation:

$$
\begin{aligned}
&\mathscr{L}'_0(\boldsymbol{\phi}, \boldsymbol{u}, p, \boldsymbol{v}_0, q_0, s_1, \hat{\boldsymbol{u}}_1, \hat{p}_1, \hat{\boldsymbol{v}}_0, \hat{q}_0)\left[\boldsymbol{\varphi}, \tilde{\boldsymbol{u}}, \tilde{p}, \tilde{\boldsymbol{v}}_0, \tilde{q}_0, \tilde{s}_1, \tilde{\hat{\boldsymbol{u}}}_1, \tilde{\hat{p}}_1, \tilde{\hat{\boldsymbol{v}}}_0, \tilde{\hat{q}}_0\right] \\
&\quad = \mathscr{L}_{0\boldsymbol{\phi}}(\boldsymbol{\phi}, \boldsymbol{u}, p, \boldsymbol{v}_0, q_0, s_1, \hat{\boldsymbol{u}}_1, \hat{p}_1, \hat{\boldsymbol{v}}_0, \hat{q}_0)[\boldsymbol{\varphi}] \\
&\qquad + \mathscr{L}_{0\boldsymbol{u},p}(\boldsymbol{\phi}, \boldsymbol{u}, p, \boldsymbol{v}_0, q_0, s_1, \hat{\boldsymbol{u}}_1, \hat{p}_1, \hat{\boldsymbol{v}}_0, \hat{q}_0)[\tilde{\boldsymbol{u}}, \tilde{p}] \\
&\qquad + \mathscr{L}_{0\boldsymbol{v}_0,q_0}(\boldsymbol{\phi}, \boldsymbol{u}, p, \boldsymbol{v}_0, q_0, s_1, \hat{\boldsymbol{u}}_1, \hat{p}_1, \hat{\boldsymbol{v}}_0, \hat{q}_0)[\tilde{\boldsymbol{v}}_0, \tilde{q}_0] \\
&\qquad + \mathscr{L}_{0s_1}(\boldsymbol{\phi}, \boldsymbol{u}, p, \boldsymbol{v}_0, q_0, s_1, \hat{\boldsymbol{u}}_1, \hat{p}_1, \hat{\boldsymbol{v}}_0, \hat{q}_0)[\tilde{s}_1] \\
&\qquad + \mathscr{L}_{0\hat{\boldsymbol{u}}_1,\hat{p}_1}(\boldsymbol{\phi}, \boldsymbol{u}, p, \boldsymbol{v}_0, q_0, s_1, \hat{\boldsymbol{u}}_1, \hat{p}_1, \hat{\boldsymbol{v}}_0, \hat{q}_0)\left[\tilde{\hat{\boldsymbol{u}}}_1, \tilde{\hat{p}}_1\right] \\
&\qquad + \mathscr{L}_{0\hat{\boldsymbol{v}}_0,\hat{q}_0}(\boldsymbol{\phi}, \boldsymbol{u}, p, \boldsymbol{v}_0, q_0, s_1, \hat{\boldsymbol{u}}_1, \hat{p}_1, \hat{\boldsymbol{v}}_0, \hat{q}_0)\left[\tilde{\hat{\boldsymbol{v}}}_0, \tilde{\hat{q}}_0\right] \\
&\qquad \forall \left(\boldsymbol{\varphi}, \tilde{\boldsymbol{u}}, \tilde{p}, \tilde{\boldsymbol{v}}_0, \tilde{q}_0, \tilde{s}_1, \tilde{\hat{\boldsymbol{u}}}_1, \tilde{\hat{p}}_1, \tilde{\hat{\boldsymbol{v}}}_0, \tilde{\hat{q}}_0\right) \in X \times (U \times P)^2 \times \mathbb{C} \times \left(\hat{U} \times \hat{P}\right)^2
\end{aligned} \tag{18}
$$

as defined in (3) and (5). The details of each term are shown below.

The third and sixth terms on the right-hand side of (18) become

$$
\begin{aligned}
&\mathscr{L}_{0\boldsymbol{v}_0,q_0}(\boldsymbol{\phi}, \boldsymbol{u}, p, \boldsymbol{v}_0, q_0, s_1, \hat{\boldsymbol{u}}_1, \hat{p}_1, \hat{\boldsymbol{v}}_0, \hat{q}_0)[\tilde{\boldsymbol{v}}_0, \tilde{q}_0] \\
&\quad = -\mathscr{L}_{\mathrm{S}\boldsymbol{v}_0,q_0}(\boldsymbol{\phi}, \boldsymbol{u}, p, \boldsymbol{v}_0, q_0)[\tilde{\boldsymbol{v}}_0, \tilde{q}_0] = -\mathscr{L}_{\mathrm{S}}(\boldsymbol{\phi}, \boldsymbol{u}, p, \tilde{\boldsymbol{v}}_0, \tilde{q}_0),
\end{aligned} \tag{19}
$$

$$
\begin{aligned}
&\mathscr{L}_{0\hat{\boldsymbol{v}}_0,\hat{q}_0}(\boldsymbol{\phi}, \boldsymbol{u}, p, \boldsymbol{v}_0, q_0, s_1, \hat{\boldsymbol{u}}_1, \hat{p}_1, \hat{\boldsymbol{v}}_0, \hat{q}_0)\left[\tilde{\hat{\boldsymbol{v}}}_0, \tilde{\hat{q}}_0\right] \\
&\quad = -\hat{\mathscr{L}}_{\mathrm{S}\hat{\boldsymbol{v}}_0,\hat{q}_0}(\boldsymbol{\phi}, s_1, \boldsymbol{u}, \hat{\boldsymbol{u}}_1, \hat{p}_1, \hat{\boldsymbol{v}}_0, \hat{q}_0)\left[\tilde{\hat{\boldsymbol{v}}}_0, \tilde{\hat{q}}_0\right] = -\hat{\mathscr{L}}_{\mathrm{S}}\left(\boldsymbol{\phi}, s_1, \boldsymbol{u}, \hat{\boldsymbol{u}}_1, \hat{p}_1, \tilde{\hat{\boldsymbol{v}}}_0, \tilde{\hat{q}}_0\right),
\end{aligned} \tag{20}
$$

respectively. (19) and (20) accord with the Lagrange functions of Problems 3.1 and 3.2. Hence, if $(\boldsymbol{u}, p)$ and $(s_1, \hat{\boldsymbol{u}}_1, \hat{p}_1)$ are the weak solutions of these problems, the third and sixth terms of (18) become 0.

The fifth term on the right-hand side of (18) becomes

$$
\begin{aligned}
&\mathscr{L}_{0\hat{\boldsymbol{u}}_1,\hat{p}_1}(\boldsymbol{\phi}, \boldsymbol{u}, p, \boldsymbol{v}_0, q_0, s_1, \hat{\boldsymbol{u}}_1, \hat{p}_1, \hat{\boldsymbol{v}}_0, \hat{q}_0)\left[\tilde{\hat{\boldsymbol{u}}}_1, \tilde{\hat{p}}_1\right] \\
&\quad = -2\mathrm{Real}\Big[\int_{\Omega(\boldsymbol{\phi})}\Big[-\rho s_1 \tilde{\hat{\boldsymbol{u}}}_1 \cdot \hat{\boldsymbol{v}}_0^{\mathrm{c}} - \rho\left\{(\boldsymbol{u}\cdot\boldsymbol{\nabla})\,\tilde{\hat{\boldsymbol{u}}}_1\right\}\cdot\hat{\boldsymbol{v}}_0^{\mathrm{c}} - \rho\left\{\left(\tilde{\hat{\boldsymbol{u}}}_1\cdot\boldsymbol{\nabla}\right)\boldsymbol{u}\right\}\cdot\hat{\boldsymbol{v}}_0^{\mathrm{c}} \\
&\qquad\qquad - \mu\left(\boldsymbol{\nabla}\tilde{\hat{\boldsymbol{u}}}_1^{\mathrm{T}}\right)\cdot\left(\boldsymbol{\nabla}\hat{\boldsymbol{v}}_0^{\mathrm{c}\mathrm{T}}\right) + \tilde{\hat{p}}_1\boldsymbol{\nabla}\cdot\hat{\boldsymbol{v}}_0^{\mathrm{c}} + \hat{q}_0^{\mathrm{c}}\boldsymbol{\nabla}\cdot\tilde{\hat{\boldsymbol{u}}}_1\Big]\mathrm{d}x \\
&\qquad + \int_{\Gamma_{\mathrm{D}}(\boldsymbol{\phi})}\left\{\tilde{\hat{\boldsymbol{u}}}_1\cdot(\mu\partial_\nu\hat{\boldsymbol{v}}_0^{\mathrm{c}} - \hat{q}_0^{\mathrm{c}}\boldsymbol{\nu}) + \hat{\boldsymbol{v}}_0^{\mathrm{c}}\cdot\left(\mu\partial_\nu\tilde{\hat{\boldsymbol{u}}}_1 - \tilde{\hat{p}}_1\boldsymbol{\nu}\right)\right\}\mathrm{d}\gamma\Big] \\
&\quad = -2\mathrm{Real}\Big[\int_{\Omega(\boldsymbol{\phi})}\Big[-\rho s_1 \tilde{\hat{\boldsymbol{u}}}_1 \cdot \hat{\boldsymbol{v}}_0^{\mathrm{c}} + \rho\left\{(\boldsymbol{u}\cdot\boldsymbol{\nabla})\,\hat{\boldsymbol{v}}_0^{\mathrm{c}}\right\}\cdot\tilde{\hat{\boldsymbol{u}}}_1 - \rho\left\{\left(\boldsymbol{\nabla}\boldsymbol{u}^{\mathrm{T}}\right)\hat{\boldsymbol{v}}_0^{\mathrm{c}}\right\}\cdot\tilde{\hat{\boldsymbol{u}}}_1 \\
&\qquad\qquad - \mu\left(\boldsymbol{\nabla}\tilde{\hat{\boldsymbol{u}}}_1^{\mathrm{T}}\right)\cdot\left(\boldsymbol{\nabla}\hat{\boldsymbol{v}}_0^{\mathrm{c}\mathrm{T}}\right) + \tilde{\hat{p}}_1\boldsymbol{\nabla}\cdot\hat{\boldsymbol{v}}_0^{\mathrm{c}} + \hat{q}_0^{\mathrm{c}}\boldsymbol{\nabla}\cdot\tilde{\hat{\boldsymbol{u}}}_1\Big]\mathrm{d}x \\
&\qquad + \int_{\Gamma_{\mathrm{D}}(\boldsymbol{\phi})}\left\{\tilde{\hat{\boldsymbol{u}}}_1\cdot(\mu\partial_\nu\hat{\boldsymbol{v}}_0^{\mathrm{c}} - \hat{q}_0^{\mathrm{c}}\boldsymbol{\nu}) + \hat{\boldsymbol{v}}_0^{\mathrm{c}}\cdot\left(\mu\partial_\nu\tilde{\hat{\boldsymbol{u}}}_1 - \tilde{\hat{p}}_1\boldsymbol{\nu}\right) - \rho\left(\tilde{\hat{\boldsymbol{u}}}_1\cdot\hat{\boldsymbol{v}}_0^{\mathrm{c}}\right)(\boldsymbol{u}\cdot\boldsymbol{\nu})\right\}\mathrm{d}\gamma
\end{aligned}
$$

$$+\int_{\Gamma_{\mathrm{N}}(\boldsymbol{\phi})} -\rho\left(\tilde{\hat{\boldsymbol{u}}}_1\cdot\hat{\boldsymbol{v}}_0^{\mathrm{c}}\right)(\boldsymbol{u}\cdot\boldsymbol{\nu})\,\mathrm{d}\gamma\Big]. \tag{21}$$

In the second equality in (21), we used the following identities:

$$\begin{aligned}
&\int_{\Omega(\boldsymbol{\phi})}\rho\left\{\left(\tilde{\hat{\boldsymbol{u}}}_1\cdot\boldsymbol{\nabla}\right)\boldsymbol{u}\right\}\cdot\hat{\boldsymbol{v}}_0^{\mathrm{c}}\mathrm{d}x\\
&\quad=\int_{\Omega(\boldsymbol{\phi})}\rho\left\{\left(\boldsymbol{\nabla}\boldsymbol{u}^{\mathrm{T}}\right)^{\mathrm{T}}\tilde{\hat{\boldsymbol{u}}}_1\right\}\cdot\hat{\boldsymbol{v}}_0^{\mathrm{c}}\mathrm{d}x=\int_{\Omega(\boldsymbol{\phi})}\rho\left\{\left(\boldsymbol{\nabla}\boldsymbol{u}^{\mathrm{T}}\right)\hat{\boldsymbol{v}}_0^{\mathrm{c}}\right\}\cdot\tilde{\hat{\boldsymbol{u}}}_1\mathrm{d}x, \qquad (22)\\
&\int_{\Omega(\boldsymbol{\phi})}\rho\left\{(\boldsymbol{u}\cdot\boldsymbol{\nabla})\,\tilde{\hat{\boldsymbol{u}}}_1\right\}\cdot\hat{\boldsymbol{v}}_0^{\mathrm{c}}\mathrm{d}x\\
&\quad=\int_{\Omega(\boldsymbol{\phi})}\rho\left[\left\{\boldsymbol{\nabla}\left(\tilde{\hat{\boldsymbol{u}}}_1\cdot\hat{\boldsymbol{v}}_0^{\mathrm{c}}\right)\right\}\cdot\boldsymbol{u}-\left\{(\boldsymbol{u}\cdot\boldsymbol{\nabla})\,\hat{\boldsymbol{v}}_0^{\mathrm{c}}\right\}\cdot\tilde{\hat{\boldsymbol{u}}}_1\right]\mathrm{d}x\\
&\quad=\int_{\partial\Omega(\boldsymbol{\phi})}\rho\left(\tilde{\hat{\boldsymbol{u}}}_1\cdot\hat{\boldsymbol{v}}_0^{\mathrm{c}}\right)(\boldsymbol{u}\cdot\boldsymbol{\nu})\,\mathrm{d}\gamma-\int_{\Omega(\boldsymbol{\phi})}\rho\left[\left(\tilde{\hat{\boldsymbol{u}}}_1\cdot\hat{\boldsymbol{v}}_0^{\mathrm{c}}\right)(\boldsymbol{\nabla}\cdot\boldsymbol{u})+\left\{(\boldsymbol{u}\cdot\boldsymbol{\nabla})\,\hat{\boldsymbol{v}}_0^{\mathrm{c}}\right\}\cdot\tilde{\hat{\boldsymbol{u}}}_1\right]\mathrm{d}x\\
&\quad=\int_{\partial\Omega(\boldsymbol{\phi})}\rho\left(\tilde{\hat{\boldsymbol{u}}}_1\cdot\hat{\boldsymbol{v}}_0^{\mathrm{c}}\right)(\boldsymbol{u}\cdot\boldsymbol{\nu})\,\mathrm{d}\gamma-\int_{\Omega(\boldsymbol{\phi})}\rho\left\{(\boldsymbol{u}\cdot\boldsymbol{\nabla})\,\hat{\boldsymbol{v}}_0^{\mathrm{c}}\right\}\cdot\tilde{\hat{\boldsymbol{u}}}_1\mathrm{d}x. \qquad (23)
\end{aligned}$$

The part of the first integral on the right-hand side of (21) with the fourth to sixth terms of the integrand becomes

$$\begin{aligned}
&\int_{\Omega(\boldsymbol{\phi})}\left[-\mu\left(\boldsymbol{\nabla}\tilde{\hat{\boldsymbol{u}}}_1^{\mathrm{T}}\right)\cdot\left(\boldsymbol{\nabla}\hat{\boldsymbol{v}}_0^{\mathrm{cT}}\right)+\tilde{\hat{p}}_1\boldsymbol{\nabla}\cdot\hat{\boldsymbol{v}}_0^{\mathrm{c}}+\hat{q}_0^{\mathrm{c}}\boldsymbol{\nabla}\cdot\tilde{\hat{\boldsymbol{u}}}_1\right]\mathrm{d}x\\
&\quad=-\int_{\Gamma_{\mathrm{D}}(\boldsymbol{\phi})}\tilde{\hat{\boldsymbol{u}}}_1\cdot(\mu\partial_\nu\hat{\boldsymbol{v}}_0^{\mathrm{c}}-\hat{q}_0^{\mathrm{c}}\boldsymbol{\nu})\,\mathrm{d}\gamma-\int_{\Gamma_{\mathrm{N}}(\boldsymbol{\phi})}\tilde{\hat{\boldsymbol{u}}}_1\cdot(\mu\partial_\nu\hat{\boldsymbol{v}}_0^{\mathrm{c}}-\hat{q}_0^{\mathrm{c}}\boldsymbol{\nu})\,\mathrm{d}\gamma\\
&\qquad+\int_{\Omega(\boldsymbol{\phi})}\left[\left\{\boldsymbol{\nabla}^{\mathrm{T}}\left(\mu\boldsymbol{\nabla}\hat{\boldsymbol{v}}_0^{\mathrm{cT}}\right)-\boldsymbol{\nabla}\hat{q}_0^{\mathrm{c}}\right\}\cdot\tilde{\hat{\boldsymbol{u}}}_1+\tilde{\hat{p}}_1\boldsymbol{\nabla}\cdot\hat{\boldsymbol{v}}_0^{\mathrm{c}}\right]\mathrm{d}x. \qquad (24)
\end{aligned}$$

By substituting (24) into (21), we obtain

$$\begin{aligned}
&\mathscr{L}_{0\hat{\boldsymbol{u}}_1,\hat{p}_1}\left(\boldsymbol{\phi},\boldsymbol{u},p,\boldsymbol{v}_0,q_0,s_1,\hat{\boldsymbol{u}}_1,\hat{p}_1,\hat{\boldsymbol{v}}_0,\hat{q}_0\right)\left[\tilde{\hat{\boldsymbol{u}}}_1,\tilde{\hat{p}}_1\right]\\
&\quad=-2\mathrm{Real}\Big[\int_{\Omega(\boldsymbol{\phi})}\Big[\left\{-\rho s_1\hat{\boldsymbol{v}}_0^{\mathrm{c}}+\rho\left(\boldsymbol{u}\cdot\boldsymbol{\nabla}\right)\hat{\boldsymbol{v}}_0^{\mathrm{c}}-\rho\left(\boldsymbol{\nabla}\boldsymbol{u}^{\mathrm{T}}\right)\hat{\boldsymbol{v}}_0^{\mathrm{c}}+\boldsymbol{\nabla}^{\mathrm{T}}\left(\mu\boldsymbol{\nabla}\hat{\boldsymbol{v}}_0^{\mathrm{cT}}\right)-\boldsymbol{\nabla}\hat{q}_0^{\mathrm{c}}\right\}\cdot\tilde{\hat{\boldsymbol{u}}}_1\\
&\qquad\qquad+\tilde{\hat{p}}_1\boldsymbol{\nabla}\cdot\hat{\boldsymbol{v}}_0^{\mathrm{c}}\Big]\mathrm{d}x\\
&\qquad+\int_{\Gamma_{\mathrm{D}}(\boldsymbol{\phi})}\hat{\boldsymbol{v}}_0^{\mathrm{c}}\cdot\left\{\mu\partial_\nu\tilde{\hat{\boldsymbol{u}}}_1-\tilde{\hat{p}}_1\boldsymbol{\nu}-\rho\tilde{\hat{\boldsymbol{u}}}_1\left(\boldsymbol{u}\cdot\boldsymbol{\nu}\right)\right\}\mathrm{d}\gamma\\
&\qquad-\int_{\Gamma_{\mathrm{N}}(\boldsymbol{\phi})}\tilde{\hat{\boldsymbol{u}}}_1\cdot\left\{\mu\partial_\nu\hat{\boldsymbol{v}}_0^{\mathrm{c}}-\hat{q}_0^{\mathrm{c}}\boldsymbol{\nu}+\rho\hat{\boldsymbol{v}}_0^{\mathrm{c}}\left(\boldsymbol{u}\cdot\boldsymbol{\nu}\right)\right\}\mathrm{d}\gamma\Big]. \qquad (25)
\end{aligned}$$

Moreover, the fourth term on the right-hand side of (18) becomes

$$\mathscr{L}_{0s_1}\left(\boldsymbol{\phi},\boldsymbol{u},p,\boldsymbol{v}_0,q_0,s_1,\hat{\boldsymbol{u}}_1,\hat{p}_1,\hat{\boldsymbol{v}}_0,\hat{q}_0\right)\left[\tilde{s}_1\right]=2\mathrm{Real}\left[\tilde{s}_1\left(1+\int_{\Omega(\boldsymbol{\phi})}\rho\hat{\boldsymbol{u}}_1\cdot\hat{\boldsymbol{v}}_0^{\mathrm{c}}\right)\,\mathrm{d}x\right]. \tag{26}$$

We observe that (25) and (26) are the Lagrange function and a normalisation condition of the following complex eigenvalue problem, whose eigenvalue accords with s_1. Hence, if $(\hat{\boldsymbol{v}}_0, \hat{q}_0)$ is the weak solution of the problem, the sum of the fourth and fifth terms on the right-hand side of (18) becomes 0.

Problem 5.1 (Adjoint linear disturbance eigenvalue problem with respect to f_0)**.** *When the solution $\boldsymbol{u}$ of Problem 3.1 and the solution s_1 of Problem 3.2 are given, find $(\hat{\boldsymbol{v}}_0, \hat{q}_0) \in \hat{U} \times \hat{P}$ such that*

$$\begin{aligned}
\rho s_1 \hat{\boldsymbol{v}}_0^{\mathrm{c}} - \rho\left(\boldsymbol{u}\cdot\boldsymbol{\nabla}\right)\hat{\boldsymbol{v}}_0^{\mathrm{c}} + \rho\left(\boldsymbol{\nabla}\boldsymbol{u}^{\mathrm{T}}\right)\hat{\boldsymbol{v}}_0^{\mathrm{c}} - \left\{\boldsymbol{\nabla}^{\mathrm{T}}\left(\mu\boldsymbol{\nabla}\hat{\boldsymbol{v}}_0^{\mathrm{c}\mathrm{T}}\right)\right\}^{\mathrm{T}} + \boldsymbol{\nabla}\hat{q}_0^{\mathrm{c}} &= \boldsymbol{0}_{\mathbb{C}^d} \quad \textit{in } \Omega(\boldsymbol{\phi}), \\
\boldsymbol{\nabla}\cdot\hat{\boldsymbol{v}}_0^{\mathrm{c}} &= 0 \quad \textit{in } \Omega(\boldsymbol{\phi}), \\
\hat{\boldsymbol{v}}_0 &= \boldsymbol{0}_{\mathbb{C}^d} \quad \textit{on } \Gamma_{\mathrm{D}}(\boldsymbol{\phi}), \\
\rho\hat{\boldsymbol{v}}_0^{\mathrm{c}}\left(\boldsymbol{u}\cdot\boldsymbol{\nu}\right) + \mu\partial_\nu\hat{\boldsymbol{v}}_0^{\mathrm{c}} - \hat{q}_0^{\mathrm{c}}\boldsymbol{\nu} &= \boldsymbol{0}_{\mathbb{C}^d} \quad \textit{on } \Gamma_{\mathrm{N}}(\boldsymbol{\phi}), \\
\int_{\Omega(\boldsymbol{\phi})} \rho\hat{\boldsymbol{u}}_1\cdot\hat{\boldsymbol{v}}_0^{\mathrm{c}}\,\mathrm{d}x &= -1.
\end{aligned}$$

By comparing Problem 5.1 to Problem 3.2, it is observed that the signs of the advection terms $-\rho\left(\boldsymbol{u}\cdot\boldsymbol{\nabla}\right)\hat{\boldsymbol{v}}_0^{\mathrm{c}}$ and $\rho\left(\boldsymbol{u}\cdot\boldsymbol{\nabla}\right)\hat{\boldsymbol{u}}_r^{\mathrm{T}}$ are different, and that the self-adjoint condition does not hold.

Then, the second term on the right-hand side of (18) becomes

$$\begin{aligned}
&\mathscr{L}_{0\boldsymbol{u},p}\left(\boldsymbol{\phi},\boldsymbol{u},p,\boldsymbol{v}_0,q_0,s_1,\hat{\boldsymbol{u}}_1,\hat{p}_1,\hat{\boldsymbol{v}}_0,\hat{q}_0\right)[\tilde{\boldsymbol{u}},\tilde{p}] \\
&\quad= -\int_{\Omega(\boldsymbol{\phi})}\Big[-\rho\left\{\left(\boldsymbol{u}\cdot\boldsymbol{\nabla}\right)\tilde{\boldsymbol{u}}\right\}\cdot\boldsymbol{v}_0 - \rho\left\{\left(\tilde{\boldsymbol{u}}\cdot\boldsymbol{\nabla}\right)\boldsymbol{u}\right\}\cdot\boldsymbol{v}_0 \\
&\qquad\qquad - \mu\left(\boldsymbol{\nabla}\tilde{\boldsymbol{u}}^{\mathrm{T}}\right)\cdot\left(\boldsymbol{\nabla}\boldsymbol{v}_0^{\mathrm{T}}\right) + \tilde{p}\boldsymbol{\nabla}\cdot\boldsymbol{v}_0 + q_0\boldsymbol{\nabla}\cdot\tilde{\boldsymbol{u}} \\
&\qquad\qquad + 2\mathrm{Real}\left[-\rho\left\{\left(\tilde{\boldsymbol{u}}\cdot\boldsymbol{\nabla}\right)\hat{\boldsymbol{u}}_1\right\}\cdot\hat{\boldsymbol{v}}_0^{\mathrm{c}} - \rho\left\{\left(\hat{\boldsymbol{u}}_1\cdot\boldsymbol{\nabla}\right)\tilde{\boldsymbol{u}}\right\}\cdot\hat{\boldsymbol{v}}_0^{\mathrm{c}}\right]\Big]\mathrm{d}x \\
&\qquad - \int_{\Gamma_{\mathrm{D}}(\boldsymbol{\phi})}\left\{\tilde{\boldsymbol{u}}\cdot\left(\mu\partial_\nu\boldsymbol{v}_0 - q_0\boldsymbol{\nu}\right) + \boldsymbol{v}_0\cdot\left(\mu\partial_\nu\tilde{\boldsymbol{u}} - \tilde{p}\boldsymbol{\nu}\right)\right\}\mathrm{d}\gamma \\
&\quad= -\int_{\Omega(\boldsymbol{\phi})}\Big[\rho\left\{\left(\boldsymbol{u}\cdot\boldsymbol{\nabla}\right)\boldsymbol{v}_0\right\}\cdot\tilde{\boldsymbol{u}} - \rho\left\{\left(\boldsymbol{\nabla}\boldsymbol{u}^{\mathrm{T}}\right)\boldsymbol{v}_0\right\}\cdot\tilde{\boldsymbol{u}} \\
&\qquad\qquad - \mu\left(\boldsymbol{\nabla}\tilde{\boldsymbol{u}}^{\mathrm{T}}\right)\cdot\left(\boldsymbol{\nabla}\boldsymbol{v}_0^{\mathrm{T}}\right) + \tilde{p}\boldsymbol{\nabla}\cdot\boldsymbol{v}_0 + q_0\boldsymbol{\nabla}\cdot\tilde{\boldsymbol{u}} \\
&\qquad\qquad + 2\mathrm{Real}\left[\rho\left\{\left(\hat{\boldsymbol{u}}_1\cdot\boldsymbol{\nabla}\right)\hat{\boldsymbol{v}}_0^{\mathrm{c}}\right\}\cdot\tilde{\boldsymbol{u}} - \rho\left\{\left(\boldsymbol{\nabla}\hat{\boldsymbol{u}}_1^{\mathrm{T}}\right)\hat{\boldsymbol{v}}_0^{\mathrm{c}}\right\}\cdot\tilde{\boldsymbol{u}}\right]\Big]\mathrm{d}x \\
&\qquad - \int_{\Gamma_{\mathrm{D}}(\boldsymbol{\phi})}\Big\{\tilde{\boldsymbol{u}}\cdot\left(\mu\partial_\nu\boldsymbol{v}_0 - q_0\boldsymbol{\nu}\right) + \boldsymbol{v}_0\cdot\left(\mu\partial_\nu\tilde{\boldsymbol{u}} - \tilde{p}\boldsymbol{\nu}\right) - \rho\left(\tilde{\boldsymbol{u}}\cdot\boldsymbol{v}_0\right)\left(\boldsymbol{u}\cdot\boldsymbol{\nu}\right) \\
&\qquad\qquad - 2\mathrm{Real}\left[\rho\left(\tilde{\boldsymbol{u}}\cdot\hat{\boldsymbol{v}}_0^{\mathrm{c}}\right)\left(\hat{\boldsymbol{u}}_1\cdot\boldsymbol{\nu}\right)\right]\Big\}\mathrm{d}\gamma \\
&\qquad - \int_{\Gamma_{\mathrm{N}}(\boldsymbol{\phi})}\left\{-\rho\left(\tilde{\boldsymbol{u}}\cdot\boldsymbol{v}_0\right)\left(\boldsymbol{u}\cdot\boldsymbol{\nu}\right) - 2\mathrm{Real}\left[\rho\left(\tilde{\boldsymbol{u}}\cdot\hat{\boldsymbol{v}}_0^{\mathrm{c}}\right)\left(\hat{\boldsymbol{u}}_1\cdot\boldsymbol{\nu}\right)\right]\right\}\mathrm{d}\gamma. \qquad (27)
\end{aligned}$$

Here, the identities of (22) and (23) were used. Moreover, the part of the first integral on the right-hand side of (27) with the third to fifth terms of the integrand becomes

$$\int_{\Omega(\boldsymbol{\phi})}\left[-\mu\left(\boldsymbol{\nabla}\tilde{\boldsymbol{u}}^{\mathrm{T}}\right)\cdot\left(\boldsymbol{\nabla}\boldsymbol{v}_0^{\mathrm{T}}\right) + \tilde{p}\boldsymbol{\nabla}\cdot\boldsymbol{v}_0 + q_0\boldsymbol{\nabla}\cdot\tilde{\boldsymbol{u}}\right]\mathrm{d}x$$

$$
\begin{aligned}
&= -\int_{\Gamma_{\mathrm{D}}(\boldsymbol{\phi})} \tilde{\boldsymbol{u}} \cdot (\mu \partial_\nu \boldsymbol{v}_0 - q_0 \boldsymbol{\nu}) \, \mathrm{d}\gamma - \int_{\Gamma_{\mathrm{N}}(\boldsymbol{\phi})} \tilde{\boldsymbol{u}} \cdot (\mu \partial_\nu \boldsymbol{v}_0 - q_0 \boldsymbol{\nu}) \, \mathrm{d}\gamma \\
&+ \int_{\Omega(\boldsymbol{\phi})} \left[\left\{ \boldsymbol{\nabla}^{\mathrm{T}} \left(\mu \boldsymbol{\nabla} \boldsymbol{v}_0^{\mathrm{T}} \right) - \boldsymbol{\nabla} q_0 \right\} \cdot \tilde{\boldsymbol{u}} + \tilde{p} \boldsymbol{\nabla} \cdot \boldsymbol{v}_0 \right] \mathrm{d}x. \qquad (28)
\end{aligned}
$$

By substituting (28) into (27), we obtain:

$$
\begin{aligned}
&\mathscr{L}_{0\boldsymbol{u},p} (\boldsymbol{\phi}, \boldsymbol{u}, p, \boldsymbol{v}_0, q_0, s_1, \hat{\boldsymbol{u}}_1, \hat{p}_1, \hat{\boldsymbol{v}}_0, \hat{q}_0) [\tilde{\boldsymbol{u}}, \tilde{p}] \\
&= -\int_{\Omega(\boldsymbol{\phi})} \Bigg[\Big\{ \rho (\boldsymbol{u} \cdot \boldsymbol{\nabla}) \boldsymbol{v}_0 - \rho \left(\boldsymbol{\nabla} \boldsymbol{u}^{\mathrm{T}} \right) \boldsymbol{v}_0 + \boldsymbol{\nabla}^{\mathrm{T}} \left(\mu \boldsymbol{\nabla} \boldsymbol{v}_0^{\mathrm{T}} \right) - \boldsymbol{\nabla} q_0 \\
&\qquad + 2\mathrm{Real} \left[\rho (\hat{\boldsymbol{u}}_1 \cdot \boldsymbol{\nabla}) \hat{\boldsymbol{v}}_0^{\mathrm{c}} - \rho \left(\boldsymbol{\nabla} \hat{\boldsymbol{u}}_1^{\mathrm{T}} \right) \hat{\boldsymbol{v}}_0^{\mathrm{c}} \right] \Big\} \cdot \tilde{\boldsymbol{u}} + q_0 \boldsymbol{\nabla} \cdot \tilde{\boldsymbol{u}} \Bigg] \mathrm{d}x \\
&\quad - \int_{\Gamma_{\mathrm{D}}(\boldsymbol{\phi})} \boldsymbol{v}_0 \cdot \{ \nu \tilde{\boldsymbol{u}} - \tilde{p} \boldsymbol{\nu} + \rho \tilde{\boldsymbol{u}} (\boldsymbol{u} \cdot \boldsymbol{\nu}) \} - 2\mathrm{Real} \left[\hat{\boldsymbol{v}}_0^{\mathrm{c}} \cdot \rho \tilde{\boldsymbol{u}} (\hat{\boldsymbol{u}}_1 \cdot \boldsymbol{\nu}) \right] \mathrm{d}\gamma \\
&\quad + \int_{\Gamma_{\mathrm{N}}(\boldsymbol{\phi})} \tilde{\boldsymbol{u}} \cdot \{ \mu \partial_\nu \boldsymbol{v}_0 - q_0 \boldsymbol{\nu} + \rho \boldsymbol{v}_0 (\boldsymbol{u} \cdot \boldsymbol{\nu}) + 2\mathrm{Real} \left[\rho \hat{\boldsymbol{v}}_0^{\mathrm{c}} (\hat{\boldsymbol{u}}_1 \cdot \boldsymbol{\nu}) \right] \} \mathrm{d}\gamma. \qquad (29)
\end{aligned}
$$

Here, we observe that (29) is the Lagrange function of the following problem. Hence, if $(\boldsymbol{v}_0, q_0)$ is the weak solution of the problem, the second term on the right-hand side of (18) becomes 0.

Problem 5.2 (Adjoint stationary Navier–Stokes problem with respect to f_0)**.** *If the solutions $\boldsymbol{u}$ of Problem 3.1, $\hat{\boldsymbol{u}}_1$ of Problem 3.2, and $\hat{\boldsymbol{v}}_0$ of Problem 5.1 are given, find $(\boldsymbol{v}_0, q_0) \in \mathcal{S} \times \mathcal{Q}$ satisfying*

$$
\begin{aligned}
-\rho (\boldsymbol{u} \cdot \boldsymbol{\nabla}) \boldsymbol{v}_0 + \rho \left(\boldsymbol{\nabla} \boldsymbol{u}^{\mathrm{T}} \right) \boldsymbol{v}_0 - \left\{ \boldsymbol{\nabla}^{\mathrm{T}} \left(\mu \boldsymbol{\nabla} \boldsymbol{v}_0^{\mathrm{T}} \right) \right\}^{\mathrm{T}} + \boldsymbol{\nabla} q_0 & \\
= 2\mathrm{Real} \left[\rho (\hat{\boldsymbol{u}}_1 \cdot \boldsymbol{\nabla}) \hat{\boldsymbol{v}}_0^{\mathrm{c}} - \rho \left(\boldsymbol{\nabla} \hat{\boldsymbol{u}}_1^{\mathrm{T}} \right) \hat{\boldsymbol{v}}_0^{\mathrm{c}} \right] & \quad \textit{in } \Omega(\boldsymbol{\phi}), \\
\boldsymbol{\nabla} \cdot \boldsymbol{v}_0 = 0 \quad \textit{in } \Omega(\boldsymbol{\phi}), & \\
\boldsymbol{v}_0 = \boldsymbol{0}_{\mathbb{R}^d} \quad \textit{on } \Gamma_{\mathrm{D}}(\boldsymbol{\phi}), & \\
\rho \boldsymbol{v}_0 (\boldsymbol{u} \cdot \boldsymbol{\nu}) + \mu \partial_\nu \boldsymbol{v}_0 - q_0 \boldsymbol{\nu} = -2\mathrm{Real} \left[\rho \hat{\boldsymbol{v}}_0^{\mathrm{c}} (\hat{\boldsymbol{u}}_1 \cdot \boldsymbol{\nu}) \right] & \quad \textit{on } \Gamma_{\mathrm{N}}(\boldsymbol{\phi}).
\end{aligned}
$$

Problem 5.2 is a stationary Navier–Stokes problem modified in terms of body force and traction.

Moreover, the first term on the right-hand side of (18) can be written as

$$
\begin{aligned}
&\mathscr{L}_{0\boldsymbol{\phi}} (\boldsymbol{\phi}, \boldsymbol{u}, p, \boldsymbol{v}_0, q_0, s_1, \hat{\boldsymbol{u}}_1, \hat{p}_1, \hat{\boldsymbol{v}}_0, \hat{q}_0) [\boldsymbol{\varphi}] \\
&\quad = -\mathscr{L}_{\mathrm{S}\boldsymbol{\phi}} (\boldsymbol{\phi}, \boldsymbol{u}, p, \boldsymbol{v}_0, q_0) [\boldsymbol{\varphi}] - \hat{\mathscr{L}}_{\mathrm{S}\boldsymbol{\phi}} (\boldsymbol{\phi}, s_1, \boldsymbol{u}, \hat{\boldsymbol{u}}_1, \hat{p}_1, \hat{\boldsymbol{v}}_0, \hat{q}_0) [\boldsymbol{\varphi}]. \qquad (30)
\end{aligned}
$$

The first term on the right-hand side of (30) is calculated by using the formulae of (3) and (5) as

$$
\begin{aligned}
&\mathscr{L}_{\mathrm{S}\boldsymbol{\phi}} (\boldsymbol{\phi}, \boldsymbol{u}, p, \boldsymbol{v}_0, q_0) [\boldsymbol{\varphi}] \\
&\quad = \int_{\Omega(\boldsymbol{\phi})} \Big[\rho \left\{ \left(\boldsymbol{u} \cdot \left(\left(\boldsymbol{\nabla} \boldsymbol{\varphi}^{\mathrm{T}} \right) \boldsymbol{\nabla} \right) \right) \boldsymbol{u} \right\} \cdot \boldsymbol{v}_0 \\
&\qquad + \mu \left(\boldsymbol{\nabla} \boldsymbol{u}^{\mathrm{T}} \right) \cdot \left(\left(\boldsymbol{\nabla} \boldsymbol{\varphi}^{\mathrm{T}} \right) \boldsymbol{\nabla} \boldsymbol{v}_0^{\mathrm{T}} \right) + \mu \left(\boldsymbol{\nabla} \boldsymbol{v}_0^{\mathrm{T}} \right) \cdot \left(\left(\boldsymbol{\nabla} \boldsymbol{\varphi}^{\mathrm{T}} \right) \boldsymbol{\nabla} \boldsymbol{u}^{\mathrm{T}} \right)
\end{aligned}
$$

$$
\begin{aligned}
&- p\left(\left(\boldsymbol{\nabla}\boldsymbol{\varphi}^{\mathrm{T}}\right)\boldsymbol{\nabla}\right)\cdot\boldsymbol{v}_0 - q_0\left(\left(\boldsymbol{\nabla}\boldsymbol{\varphi}^{\mathrm{T}}\right)\boldsymbol{\nabla}\right)\cdot\boldsymbol{u}\\
&+\left(-\rho\left(\left(\boldsymbol{u}\cdot\boldsymbol{\nabla}\right)\boldsymbol{u}\right)\cdot\boldsymbol{v}_0 - \mu\left(\boldsymbol{\nabla}\boldsymbol{u}^{\mathrm{T}}\right)\cdot\left(\boldsymbol{\nabla}\boldsymbol{v}_0^{\mathrm{T}}\right)\right.\\
&\left.+ p\boldsymbol{\nabla}\cdot\boldsymbol{v}_0 + q_0\boldsymbol{\nabla}\cdot\boldsymbol{u} + \boldsymbol{b}\cdot\boldsymbol{v}_0\right)\boldsymbol{\nabla}\cdot\boldsymbol{\varphi}\Big]\mathrm{d}x\\
&+\int_{\Gamma_{\mathrm{D}}(\boldsymbol{\phi})}\Big[\left(\boldsymbol{u}-\boldsymbol{u}_{\mathrm{D}}\right)\cdot\boldsymbol{w}\left(\boldsymbol{\varphi},\boldsymbol{v}_0,q_0\right) + \boldsymbol{v}_0\cdot\boldsymbol{w}\left(\boldsymbol{\varphi},\boldsymbol{u},p\right)\\
&+\left\{\left(\boldsymbol{u}-\boldsymbol{u}_{\mathrm{D}}\right)\cdot\left(\mu\partial_\nu\boldsymbol{v}_0 - q_0\boldsymbol{\nu}\right) + \boldsymbol{v}_0\cdot\left(\mu\partial_\nu\boldsymbol{u} - p\boldsymbol{\nu}\right)\right\}\left(\boldsymbol{\nabla}\cdot\boldsymbol{\varphi}\right)_\tau\Big]\mathrm{d}\gamma,
\end{aligned}
$$

where

$$
\boldsymbol{w}\left(\boldsymbol{\varphi},\boldsymbol{u},p\right) = \left\{\left(\mu\boldsymbol{\nabla}\boldsymbol{u}^{\mathrm{T}}\right)^{\mathrm{T}} - p\boldsymbol{I}\right\}\left[\left\{\boldsymbol{\nu}\cdot\left(\boldsymbol{\nabla}\boldsymbol{\varphi}^{\mathrm{T}}\boldsymbol{\nu}\right)\right\}\boldsymbol{\nu} - \left\{\boldsymbol{\nabla}\boldsymbol{\varphi}^{\mathrm{T}} + \left(\boldsymbol{\nabla}\boldsymbol{\varphi}^{\mathrm{T}}\right)^{\mathrm{T}}\right\}\boldsymbol{\nu}\right].
$$

Moreover, the second term on the right-hand side of (30) becomes

$$
\begin{aligned}
&\hat{\mathscr{L}}_{\mathrm{S}\boldsymbol{\phi}}\left(\boldsymbol{\phi},s_1,\boldsymbol{u},\hat{\boldsymbol{u}}_1,\hat{p}_1,\hat{\boldsymbol{v}}_0,\hat{q}_0\right)[\boldsymbol{\varphi}]\\
&\quad=\int_{\Omega(\boldsymbol{\phi})}2\mathrm{Real}\Big[\rho\left\{\left(\boldsymbol{u}\cdot\left(\left(\boldsymbol{\nabla}\boldsymbol{\varphi}^{\mathrm{T}}\right)\boldsymbol{\nabla}\right)\right)\hat{\boldsymbol{u}}_1\right\}\cdot\hat{\boldsymbol{v}}_0^{\mathrm{c}} + \rho\left\{\left(\hat{\boldsymbol{u}}_1\cdot\left(\left(\boldsymbol{\nabla}\boldsymbol{\varphi}^{\mathrm{T}}\right)\boldsymbol{\nabla}\right)\right)\boldsymbol{u}\right\}\cdot\hat{\boldsymbol{v}}_0^{\mathrm{c}}\\
&\qquad+\mu\left(\boldsymbol{\nabla}\hat{\boldsymbol{u}}_1^{\mathrm{T}}\right)\cdot\left\{\left(\boldsymbol{\nabla}\boldsymbol{\varphi}^{\mathrm{T}}\right)\boldsymbol{\nabla}\hat{\boldsymbol{v}}_0^{\mathrm{cT}}\right\} + \mu\left(\boldsymbol{\nabla}\hat{\boldsymbol{v}}_0^{\mathrm{cT}}\right)\cdot\left\{\left(\boldsymbol{\nabla}\boldsymbol{\varphi}^{\mathrm{T}}\right)\boldsymbol{\nabla}\hat{\boldsymbol{u}}_1^{\mathrm{T}}\right\}\\
&\qquad-\hat{p}_1\left(\left(\boldsymbol{\nabla}\boldsymbol{\varphi}^{\mathrm{T}}\right)\boldsymbol{\nabla}\right)\cdot\hat{\boldsymbol{v}}_0^{\mathrm{c}} - \hat{q}_0^{\mathrm{c}}\left(\left(\boldsymbol{\nabla}\boldsymbol{\varphi}^{\mathrm{T}}\right)\boldsymbol{\nabla}\right)\cdot\hat{\boldsymbol{u}}_1\\
&\qquad+\Big\{-\rho s_1\hat{\boldsymbol{u}}_1\cdot\hat{\boldsymbol{v}}_0^{\mathrm{c}} - \rho\left(\left(\boldsymbol{u}\cdot\boldsymbol{\nabla}\right)\hat{\boldsymbol{u}}_1\right)\cdot\hat{\boldsymbol{v}}_0^{\mathrm{c}} - \rho\left(\left(\hat{\boldsymbol{u}}_1\cdot\boldsymbol{\nabla}\right)\boldsymbol{u}\right)\cdot\hat{\boldsymbol{v}}_0^{\mathrm{c}}\\
&\qquad-\mu\left(\boldsymbol{\nabla}\hat{\boldsymbol{u}}_1^{\mathrm{T}}\right)\cdot\left(\boldsymbol{\nabla}\hat{\boldsymbol{v}}_0^{\mathrm{cT}}\right) + \hat{p}_1\boldsymbol{\nabla}\cdot\hat{\boldsymbol{v}}_0^{\mathrm{c}} + \hat{q}_0^{\mathrm{c}}\boldsymbol{\nabla}\cdot\hat{\boldsymbol{u}}_1\Big\}\boldsymbol{\nabla}\cdot\boldsymbol{\varphi}\Big]\mathrm{d}x\\
&\qquad+\int_{\Gamma_{\mathrm{D}}(\boldsymbol{\phi})}2\mathrm{Real}\big[\left(\hat{\boldsymbol{u}}_1+\hat{\boldsymbol{v}}_0^{\mathrm{c}}\right)\boldsymbol{w}\left(\boldsymbol{\varphi},\boldsymbol{v}_0\right)\\
&\qquad+\left(\hat{\boldsymbol{u}}_1\cdot\left(\mu\partial_\nu\hat{\boldsymbol{v}}_0^{\mathrm{c}} - \hat{q}_0^{\mathrm{c}}\boldsymbol{\nu}\right) + \hat{\boldsymbol{v}}_0^{\mathrm{c}}\cdot\left(\mu\partial_\nu\hat{\boldsymbol{u}}_1 - \hat{p}_1\boldsymbol{\nu}\right)\right)\left(\boldsymbol{\nabla}\cdot\boldsymbol{\varphi}\right)_\tau\big]\mathrm{d}\gamma.
\end{aligned}
$$

Here, we assume that $(\boldsymbol{u},p)$, $(s_1,\hat{\boldsymbol{u}}_1,\hat{p}_1)$, $(\hat{\boldsymbol{v}}_0,\hat{q}_0)$ and $(\boldsymbol{v}_0,q_0)$ are the weak solutions of Problems 3.1, 3.2, 5.1 and 5.2, respectively. Then, by using the Dirichlet conditions, continuity equations and notation of $\tilde{f}_0\left(\boldsymbol{\phi}\right) = f_0\left(s_1\left(\boldsymbol{\phi}\right)\right)$, we obtain

$$
\begin{aligned}
&\tilde{f}_0'\left(\boldsymbol{\phi}\right)[\boldsymbol{\varphi}]\\
&\quad=\mathscr{L}_{0\boldsymbol{\phi}}\left(\boldsymbol{\phi},\boldsymbol{u},p,\boldsymbol{v}_0,q_0,s_1,\hat{\boldsymbol{u}}_1,\hat{p}_1,\hat{\boldsymbol{v}}_0,\hat{q}_0\right)[\boldsymbol{\varphi}]\\
&\quad=\int_{\Omega(\boldsymbol{\phi})}\left(\boldsymbol{G}_{\Omega 0}\cdot\left(\boldsymbol{\nabla}\boldsymbol{\varphi}^{\mathrm{T}}\right) + g_{\Omega 0}\boldsymbol{\nabla}\cdot\boldsymbol{\varphi}\right)\mathrm{d}x\\
&\quad=\left\langle\boldsymbol{g}_0,\boldsymbol{\varphi}\right\rangle,
\end{aligned}
\tag{31}
$$

where

$$
\begin{aligned}
\boldsymbol{G}_{\Omega 0} &= -\rho\left(\boldsymbol{u}\boldsymbol{v}_0^{\mathrm{T}}\right)\left(\boldsymbol{\nabla}\boldsymbol{u}^{\mathrm{T}}\right)^{\mathrm{T}} - \mu\boldsymbol{\nabla}\boldsymbol{u}^{\mathrm{T}}\left(\boldsymbol{\nabla}\boldsymbol{v}_0^{\mathrm{T}}\right)^{\mathrm{T}} - \mu\boldsymbol{\nabla}\boldsymbol{v}_0^{\mathrm{T}}\left(\boldsymbol{\nabla}\boldsymbol{u}^{\mathrm{T}}\right)^{\mathrm{T}} + p\left(\boldsymbol{\nabla}\boldsymbol{v}_0^{\mathrm{T}}\right)^{\mathrm{T}}\\
&\quad+ q_0\left(\boldsymbol{\nabla}\boldsymbol{u}^{\mathrm{T}}\right)^{\mathrm{T}} - 2\mathrm{Real}\Big[\rho\left(\boldsymbol{u}\hat{\boldsymbol{v}}_0^{\mathrm{cT}}\right)\left(\boldsymbol{\nabla}\hat{\boldsymbol{u}}_1^{\mathrm{T}}\right)^{\mathrm{T}} + \rho\left(\hat{\boldsymbol{u}}_1\hat{\boldsymbol{v}}_0^{\mathrm{cT}}\right)\left(\boldsymbol{\nabla}\boldsymbol{u}^{\mathrm{T}}\right)^{\mathrm{T}}\\
&\quad+\left(\mu\boldsymbol{\nabla}\hat{\boldsymbol{u}}_1^{\mathrm{T}} - \hat{p}_1\boldsymbol{I}\right)\left(\boldsymbol{\nabla}\hat{\boldsymbol{v}}_0^{\mathrm{cT}}\right)^{\mathrm{T}} + \left(\mu\boldsymbol{\nabla}\hat{\boldsymbol{v}}_0^{\mathrm{cT}} - \hat{q}_0^{\mathrm{c}}\boldsymbol{I}\right)\left(\boldsymbol{\nabla}\hat{\boldsymbol{u}}_1^{\mathrm{T}}\right)^{\mathrm{T}}\Big],\\
g_{\Omega 0} &= \rho\left(\left(\boldsymbol{u}\cdot\boldsymbol{\nabla}\right)\boldsymbol{u}\right)\cdot\boldsymbol{v}_0 + \mu\left(\boldsymbol{\nabla}\boldsymbol{u}^{\mathrm{T}}\right)\cdot\left(\boldsymbol{\nabla}\boldsymbol{v}_0^{\mathrm{T}}\right) - \boldsymbol{b}\cdot\boldsymbol{v}_0
\end{aligned}
\tag{32}
$$

$$
\begin{aligned}
&- 2\mathrm{Real}\Big[-\rho s_1 \hat{\boldsymbol{u}}_1 \cdot \hat{\boldsymbol{v}}_0^{\mathrm{c}} - \rho\left(\left(\boldsymbol{u}\cdot\boldsymbol{\nabla}\right)\hat{\boldsymbol{u}}_1\right)\cdot\hat{\boldsymbol{v}}_0^{\mathrm{c}} - \rho\left(\left(\hat{\boldsymbol{u}}_1\cdot\boldsymbol{\nabla}\right)\boldsymbol{u}\right)\cdot\hat{\boldsymbol{v}}_0^{\mathrm{c}} \\
&- \mu\left(\boldsymbol{\nabla}\hat{\boldsymbol{u}}_r^{\mathrm{T}}\right)\cdot\left(\boldsymbol{\nabla}\hat{\boldsymbol{v}}_0^{\mathrm{c}\mathrm{T}}\right)\Big]. \qquad (33)
\end{aligned}
$$

To obtain (32), we used

$$
\left(\boldsymbol{\nabla}\boldsymbol{\varphi}^{\mathrm{T}}\boldsymbol{\nabla}\right)\cdot\boldsymbol{v}_0 = \left(\boldsymbol{\nabla}\boldsymbol{v}_0^{\mathrm{T}}\right)^{\mathrm{T}}\cdot\boldsymbol{\nabla}\boldsymbol{\varphi}^{\mathrm{T}} = \boldsymbol{I}\cdot\left(\boldsymbol{\nabla}\boldsymbol{\varphi}^{\mathrm{T}}\boldsymbol{\nabla}\boldsymbol{v}_0^{\mathrm{T}}\right). \qquad (34)
$$

(31) is the result obtained by this study.

5.2. *Shape derivative of f_1*

Since $f_1(\boldsymbol{\phi})$ is not a functional with respect to the solutions of the state determination problems, the shape derivative of $f_1(\boldsymbol{\phi})$ is calculated by setting $u = 1$ in (3) as

$$
f_1'(\boldsymbol{\phi})[\boldsymbol{\varphi}] = \int_{\Omega(\boldsymbol{\phi})} g_{\Omega 1}\boldsymbol{\nabla}\cdot\boldsymbol{\varphi}\,\mathrm{d}x = \langle \boldsymbol{g}_1, \boldsymbol{\varphi}\rangle, \qquad (35)
$$

where

$$
g_{\Omega 1} = 1. \qquad (36)
$$

6. Numerical scheme

By using $\boldsymbol{g}_0$ and $\boldsymbol{g}_1$, we can apply an iterative algorithm based on a gradient method in X, which we call the H^1 gradient method, to solve Problem 4.1. In this section, we denote $\tilde{f}_0(\boldsymbol{\phi})$ defined in the above-mentioned (31) as $f_0(\boldsymbol{\phi})$ and consider a problem that minimises $f_0(\boldsymbol{\phi})$ under the $f_1(\boldsymbol{\phi}) \le 0$ constraint.

The H^1 gradient method for the domain variation type finds the domain variation $\boldsymbol{\varphi}_{gi} \in X$ with respect to $\boldsymbol{g}_i$ ($i \in \{0, 1\}$) as the solution to the following problem.

Problem 6.1 (H^1 gradient method of domain variation type)**.** *Let $a_X : X \times X \to \mathbb{R}$ be a bounded coercive bilinear form such that there exist $\alpha_X > 0$ and $\beta_X > 0$ satisfying*

$$
a_X(\boldsymbol{\varphi},\boldsymbol{\varphi}) \ge \alpha_X \|\boldsymbol{\varphi}\|_X^2, \quad |a_X(\boldsymbol{\varphi},\boldsymbol{\psi})| \le \beta_X \|\boldsymbol{\varphi}\|_X \|\boldsymbol{\psi}\|_X \quad \forall \boldsymbol{\varphi},\boldsymbol{\psi} \in X. \qquad (37)
$$

For $\boldsymbol{g}_i \in X'$, find $\boldsymbol{\varphi}_{gi} \in X$ such that

$$
a_X(\boldsymbol{\varphi}_{gi},\boldsymbol{\psi}) = -\langle \boldsymbol{g}_i, \boldsymbol{\psi}\rangle \quad \forall \boldsymbol{\psi} \in X. \qquad (38)
$$

The solution $\boldsymbol{\varphi}_{gi}$ decreases f_i because

$$
\begin{aligned}
&f_i(\boldsymbol{\phi}+\boldsymbol{\varphi}_{gi}) - f_i(\boldsymbol{\phi}) = \langle \boldsymbol{g}_i, \boldsymbol{\varphi}_{gi}\rangle + o\left(\|\boldsymbol{\varphi}_{gi}\|_X\right) = -\langle \boldsymbol{\varphi}_{gi}, \boldsymbol{\varphi}_{gi}\rangle + o\left(\|\boldsymbol{\varphi}_{gi}\|_X\right) \\
&\quad \le -\alpha\|\boldsymbol{\varphi}_{gi}\|_X^2 + o\left(\|\boldsymbol{\varphi}_{gi}\|_X\right)
\end{aligned}
$$

holds for a small $\boldsymbol{\varphi}_{gi}$. A simple choice for a_X is

$$
a_X(\boldsymbol{\varphi},\boldsymbol{\psi}) = \int_{\Omega(\boldsymbol{\phi})} \left\{\left(\boldsymbol{\nabla}\boldsymbol{\varphi}^{\mathrm{T}}\right)\cdot\left(\boldsymbol{\nabla}\boldsymbol{\psi}^{\mathrm{T}}\right) + c_\Omega \boldsymbol{\varphi}\cdot\boldsymbol{\psi}\right\}\mathrm{d}x, \qquad (39)
$$

where c_Ω is a positive constant to ensure that $a_X(\cdot,\cdot)$ corresponds to a coercive bilinear form, and to simultaneously control the smoothness of the solution $\boldsymbol{\varphi}_{gi}$. A lower c_Ω results in a smoother $\boldsymbol{\varphi}_{gi}$. For the regularity of $\boldsymbol{\varphi}_{gi}$, we have $\boldsymbol{\varphi}_{gi} \in \mathcal{D}$ under appropriate conditions (Azegami 2016, Theorem 9.8.6).

To solve Problem 4.1, we use an iterative method to vary the domain by using the solution $\boldsymbol{\varphi}_g$ to the following problem.

Problem 6.2 (Sequential quadratic approximation)**.** *For $\boldsymbol{\phi}_k \in \mathcal{D}$, let $\boldsymbol{g}_0$ and $\boldsymbol{g}_1$ be given, and c_a be a given positive constant to control the magnitude of $\boldsymbol{\varphi}_g$. Then, find $\boldsymbol{\varphi}_g$ such that*

$$q(\boldsymbol{\varphi}_g) = \min_{\boldsymbol{\varphi}\in X}\left\{ q(\boldsymbol{\varphi}) = \frac{c_a}{2} a_X(\boldsymbol{\varphi},\boldsymbol{\varphi}) + \langle \boldsymbol{g}_0, \boldsymbol{\varphi}\rangle \;\middle|\; f_1(\boldsymbol{\phi}_k) + \langle \boldsymbol{g}_1, \boldsymbol{\varphi}\rangle \le 0 \right\}.$$

Thereby, we can find the solution $\boldsymbol{\varphi}_g$ by defining a Lagrange function as

$$\mathscr{L}_{\mathrm{Q}}(\boldsymbol{\varphi}, \boldsymbol{\lambda}_{k+1}) = q(\boldsymbol{\varphi}) + \lambda_{1\,k+1}\left(f_1(\boldsymbol{\phi}_k) + \langle \boldsymbol{g}_1, \boldsymbol{\varphi}\rangle\right), \tag{40}$$

where $\lambda_{1\,k+1}$ are the Lagrange multipliers. The Karush–Kuhn–Tucker conditions at the minimum point $\boldsymbol{\varphi}_g$ are given as

$$c_a a_X(\boldsymbol{\varphi}_g, \boldsymbol{\varphi}) + \langle \boldsymbol{g}_0, \boldsymbol{\varphi}\rangle + \lambda_{1\,k+1}\langle \boldsymbol{g}_1, \boldsymbol{\varphi}\rangle = 0 \quad \forall \boldsymbol{\varphi} \in X, \tag{41}$$

$$f_1(\boldsymbol{\phi}_k) + \langle \boldsymbol{g}_1, \boldsymbol{\varphi}_g\rangle \le 0, \tag{42}$$

$$\lambda_{1\,k+1}\left(f_1(\boldsymbol{\phi}_k) + \langle \boldsymbol{g}_1, \boldsymbol{\varphi}_g\rangle\right) = 0, \tag{43}$$

$$\lambda_{1\,k+1} \ge 0. \tag{44}$$

Here, we assume the following form:

$$\boldsymbol{\varphi}_g = \boldsymbol{\varphi}_g(\boldsymbol{\lambda}_{k+1}) = \boldsymbol{\varphi}_{g0} + \lambda_{1\,k+1}\,\boldsymbol{\varphi}_{g1}, \tag{45}$$

where $\boldsymbol{\varphi}_{g0}$ and $\boldsymbol{\varphi}_{g1}$ are the solutions of the H^1 gradient method for each $\boldsymbol{g}_0$ and $\boldsymbol{g}_1$, respectively, obtained by

$$c_a a_X(\boldsymbol{\varphi}_{gi}, \boldsymbol{\psi}) = -\langle \boldsymbol{g}_i, \boldsymbol{\psi}\rangle \quad \forall \boldsymbol{\psi} \in X \tag{46}$$

for $i \in \{0,1\}$, and $\lambda_{1\,k+1} \in \mathbb{R}$ are unknown parameters. Then, we can find that (41) holds for $\boldsymbol{\varphi}_g$ in (45), and that (42) becomes a linear system to determine $\lambda_{1\,k+1}$, when "$\le$" is replaced by "$=$", as

$$\lambda_{1\,k+1} = -\frac{f_1(\boldsymbol{\phi}_k) + \langle \boldsymbol{g}_1, \boldsymbol{\varphi}_{g0}\rangle}{\langle \boldsymbol{g}_1, \boldsymbol{\varphi}_{g1}\rangle}. \tag{47}$$

In this case, we assume an algorithm to set $\lambda_{1\,k+1} = 0$ if $\lambda_{1\,k+1} < 0$. Then, the Karush–Kuhn–Tucker conditions are satisfied for small $\boldsymbol{\varphi}_g$. Moreover, when $f_1(\boldsymbol{\phi}_k) = 0$, $\lambda_{1\,k+1}$ is determined independently of the magnitude of $\boldsymbol{\varphi}_g$.

To control the magnitude (step size) of the search vector $\boldsymbol{\varphi}_g$ by varying c_a in (46), we use Armijo's criterion (Armijo 1966). This criterion is typically applied each time the design variable is updated. In this study, this criterion was applied to each $k_{\mathrm{I}} \in \mathbb{N}$ times, because a small oscillatory variation was observed in the iteration histories of

the objective cost function. Specifically, by letting

$$\mathscr{L}(\boldsymbol{\phi}, \lambda_1) = f_0(\boldsymbol{\phi}) + \lambda_1 f_1(\boldsymbol{\phi})$$

be the Lagrange function of the original optimisation problem with respect to Problem 6.2, we use

$$\begin{aligned} &\mathscr{L}\left(\boldsymbol{\phi}_{k-k_{\mathrm{I}}+1} + \sum_{\kappa\in\{k-k_{\mathrm{I}}+1,\ldots,k\}} \boldsymbol{\varphi}_{g\kappa}, \lambda_{1\,k+1}\right) - \mathscr{L}(\boldsymbol{\phi}_{k-k_{\mathrm{I}}+1}, \lambda_{1\,k-k_{\mathrm{I}}+1}) \\ &\quad \leq \xi \sum_{\kappa\in\{k-k_{\mathrm{I}}+1,\ldots,k\}} \langle \boldsymbol{g}_{0\kappa} + \lambda_{1\kappa}\boldsymbol{g}_{1\kappa}, \boldsymbol{\varphi}_{g\kappa}\rangle \end{aligned} \tag{48}$$

as the condition to decrease the magnitude of $\boldsymbol{\varphi}_g$, where $\xi \in (0,1)$ is a parameter to control the decreasing rate of $\mathscr{L}(\boldsymbol{\phi}, \lambda_1) \approx f_0(\boldsymbol{\phi})$.

An algorithm to solve the shape optimisation problem is presented below.

Algorithm 6.3 (Shape optimization by the H^1 gradient method)**.**

(1) Set Ω_0 and $\boldsymbol{\phi}_0 = \boldsymbol{i}$. Set c_a, ϵ_0, $\xi \in (0,1)$, k_{I} and $\alpha > 1$, appropriately, and set $k = 0$.

(2) Solve the state determination problems (Problems 3.1 and 3.2) at $\boldsymbol{\phi}_k$, and compute $f_0(\boldsymbol{\phi}_k)$ and $f_1(\boldsymbol{\phi}_k)$.

(3) Solve the adjoint problems (Problems 5.1 and 5.2) at $\boldsymbol{\phi}_k$, and compute $\boldsymbol{g}_0$ and $\boldsymbol{g}_1$.

(4) Solve $\boldsymbol{\varphi}_{g0}$ and $\boldsymbol{\varphi}_{g1}$ by using (46).

(5) Compute $\lambda_{1\,k+1}$ by using (47). When $\lambda_{1\,k+1} < 0$, replace $\lambda_{1\,k+1} = 0$.

(6) Compute $\boldsymbol{\varphi}_g$ by using (45), set $\boldsymbol{\phi}_{k+1} = \boldsymbol{\phi}_k + \boldsymbol{\varphi}_g$, and compute $f_0(\boldsymbol{\phi}_{k+1})$ and $f_1(\boldsymbol{\phi}_{k+1})$.

(7) Assess $|f_0(\boldsymbol{\phi}_{k+1}) - f_0(\boldsymbol{\phi}_k)| \leq \epsilon_0$.
- *If "Yes", proceed to (9).*
- *If "No", proceed to the next step.*

(8) If k is a multiple of k_{I}, perform the checks listed below. Otherwise, replace $k+1$ with k and return to (3).
- *If (48) is satisfied, replace $k+1$ with k and return to (3).*
- *Otherwise, substitute αc_a into c_a and $\boldsymbol{\varphi}_{g0}/c_a$, $\boldsymbol{\varphi}_{g1}/c_a$ into $\boldsymbol{\varphi}_{g0}$, $\boldsymbol{\varphi}_{g1}$, and then return to (6) of the $(k - k_{\mathrm{I}} + 1)$th iteration.*

(9) Stop the algorithm.

7. Numerical examples

Based on the scheme presented in Section 6, we developed a computer program to solve Problem 4.1 for two-dimensional flow fields with the FreeFEM++ (Hecht 2012) programming language, which implements the finite element method. Here, the Reynolds number $\mathrm{Re} = \rho v l/\mu$ is used instead of μ and ρ, where the characteristic flow velocity v and length l are shown in each example. Additionally, the used finite element models were constructed with mixed P2/P1 (Taylor Hood) finite elements.

The nonlinear problem of the stationary Navier–Stokes problem (Problem 3.1) is solved by the Newton–Raphson method. The complex eigenvalue problems of the

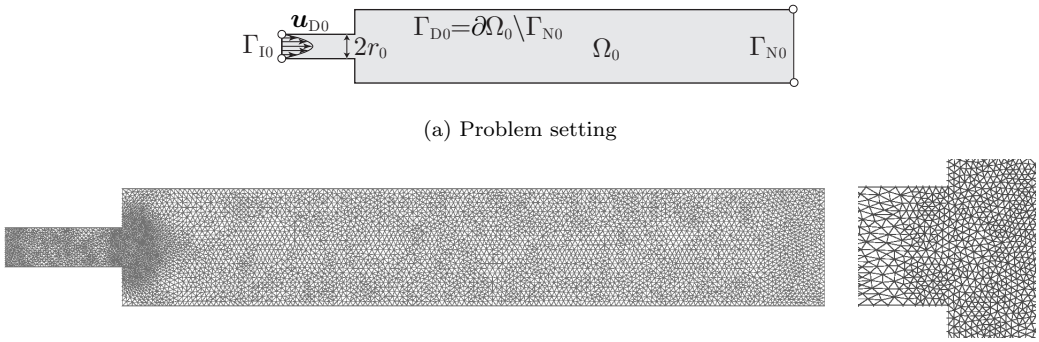

(a) Problem setting

(b) Finite element mesh

(c) Zoom of (b)

Figure 2. Poiseuille flow field with sudden expansion at initial shape.

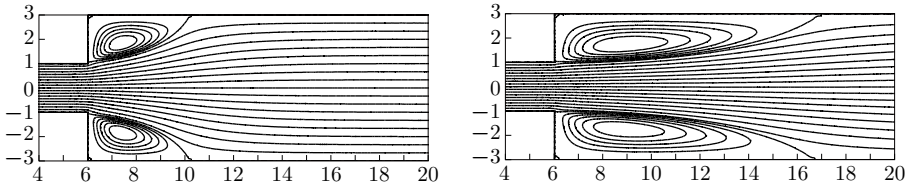

(a) Re = 15 (b) Re = 40

Figure 3. Streamlines at initial shape (Poiseuille flow field).

linear disturbance eigenvalue problem (Problem 3.2) and adjoint linear disturbance eigenvalue problem with respect to f_0 (Problem 5.1) are solved by the Arnoldi method. To solve the asymmetric sparse linear systems for the adjoint stationary Navier–Stokes problem with respect to f_0 (Problem 5.2), the H^1 gradient method (Problem 6.1) and the linear equation in the Newton–Raphson method for the stationary Navier–Stokes problem (Problem 3.1), UMFPACK (Davis 2004) were employed. In the computer program, the adaptive mesh provided in the FreeFem++ programming language was used.

In the following examples, c_1 in (17) was set with the initial domain measure in each flow field. Additionally, 1 was used with respect to the parameter c_Ω in (39). Moreover, c_a in (46) was set in each example. For the ϵ_0, ξ, and k_{I} constants used to check the convergence in Algorithm 6.3 and Armijo's criterion in (48), 10^{-4}, 10^{-4} and 5 were used, respectively. For the convergence criterion in the Newton–Raphson method, we used the following conditions:

$$\begin{aligned}\|u_{ik+1}-u_{ik}\|_{L^\infty(\Omega;\mathbb{R})} / \|u_{ik}\|_{L^\infty(\Omega;\mathbb{R})} < 10^{-6} \quad \forall i \in \{1,2\}\,,\\ \|p_{k+1}-p_k\|_{L^\infty(\Omega;\mathbb{R})} / \|p_k\|_{L^\infty(\Omega;\mathbb{R})} < 10^{-6}.\end{aligned}$$

7.1. *Poiseuille flow field with sudden expansion*

Here, we consider the Poiseuille flow field with a sudden expansion used in Nakazawa and Azegami (2016). Figure 2 shows the problem setting and initial finite element mesh. The initial domain, Reynolds number and given flow velocity are defined with $r_0 = 1$ as

$$\Omega_0 = (0,6)\times(-1,1)\cup(6,42)\times(-3,3)\,,$$

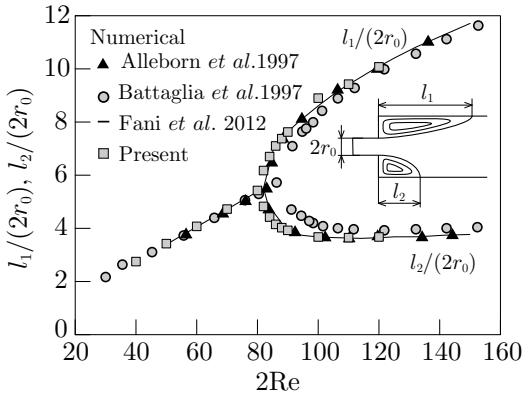

Figure 4. Vortex lengths at initial shape (Poiseuille flow field).

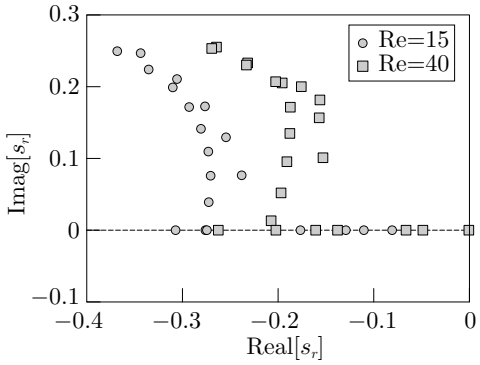

Figure 5. Distribution of eigenvalues s_r at initial shape (Poiseuille flow field).

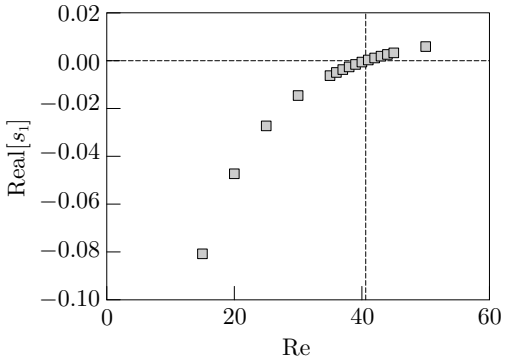

Figure 6. Change of Real $[s_1]$ with respect to Reynolds number at initial shape (Poiseuille flow field).

$$\mathrm{Re}\,(v) = \frac{\rho v r_0}{\mu}, \quad \boldsymbol{u}_{\mathrm{D}0} = v\left(1 - x_2^2, 0\right)^{\mathrm{T}} \quad \text{on } \Gamma_{\mathrm{I}0} = \left\{ (0, x_2)^{\mathrm{T}} \in \mathbb{R}^2 \;\middle|\; x_2 \in (-1, 1) \right\}.$$

The original mesh was built into the program with the format of the FreeFEM++ programming language as

```
border w1(t=0,1) { x=0; y=1-2*t; label=inflow;};
border w2(t=0,1) { x=0+6*t; y=-1; label=walld;};
border w3(t=0,1) { x=6; y=-1-2*t; label=walld;};
border w4(t=0,1) { x=6+36*t; y=-3; label=walld;};
border w5(t=0,1) { x=42; y=-3+6*t; label=outflow;};
border w6(t=0,1) { x=42-36*t; y=3; label=wallu;};
border w7(t=0,1) { x=6; y=3-2*t; label=wallu;};
border w8(t=0,1) { x=6-6*t; y=1; label=wallu;};
mesh Th = buildmesh(w1(15)+w2(45)+w3(15)+w4(150)+w5(45)+w6(150)+w7(15)+w8(45));
```

By using the adaptive mesh function with the error tolerance of err=0.003, the element number of the mesh shown in Figure 2 was 11,536. In the domain variation, $\boldsymbol{\phi} = \mathbf{0}_{\mathbb{R}^2}$ on $\Gamma_{\mathrm{I}0} \cup \Gamma_{\mathrm{N}0}$ was assumed; that is, $\bar{\Omega}_{\mathrm{C}0} = \Gamma_{\mathrm{I}0} \cup \Gamma_{\mathrm{N}0}$ in (1). For the step size parameter, $c_a = 1$ was used. In the optimisation process, the number of elements was varied from 11,000 to 12,000 by the adaptive mesh.

Figure 3 shows the streamlines in the results of the stationary Navier–Stokes problem at the initial shape, when the velocity $\boldsymbol{u}_{\mathrm{D}}$ is given as Re = 15 and 40. With respect to the lengths of the vortices, Figure 4 compares the results obtained by this study

Table 1. Comparison of critical Reynolds number (Poiseuille flow field).

Literatures	$2\mathrm{Re}_\mathrm{C}$
Battaglia et al. (1997)	80.7
Fani, Camarri, and Salvetti (2012)	81.2
Fearn, Mullin, and A. (1990)	80.9
Mizushima and Shiotani (2000)	80.46
Present study	81.2

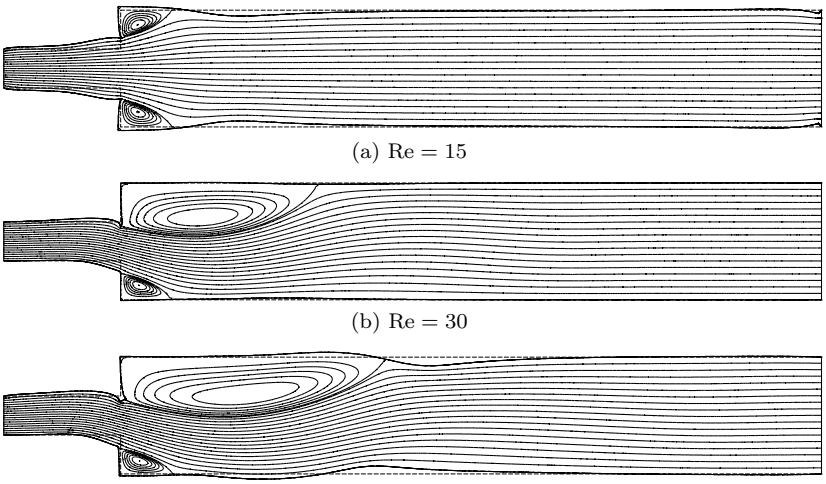

(a) Re = 15

(b) Re = 30

(c) Re = 40

Figure 7. Streamlines at optimized shape (Poiseuille flow field).

with the results obtained by Alleborn et al. (1997); Fani, Camarri, and Salvetti (2012); Battaglia et al. (1997). Moreover, the distribution of eigenvalues s_r at the initial shape is illustrated in Figure 5. In this figure, the imaginary part is neglected because the eigenvalues are complex conjugate. The first three eigenvalues were the real numbers of $s_1 = -0.0006085$, $s_2 = -0.04863$, and $s_3 = -0.06625$ when $\mathrm{Re} = 40$. Figure 6 shows the variation of $\mathrm{Real}\,[s_1]$ with respect to the Reynolds number. In the figure, the critical Reynolds number Re_C is 40.6 when $\mathrm{Real}\,[s_1] = 0$. Table 1 compares the Re_C value with the values reported in the literature. The comparison demonstrates the reliability of the analysis performed by this study.

The results of shape optimisation are shown in Figures 7–10. Figures 7 (a)–(c) illustrates the shapes and streamlines obtained by using the $\boldsymbol{u}_\mathrm{D}$ of $\mathrm{Re} = 15$, 30 and 40, respectively. In these figures, the dotted line shows the initial shapes. The iteration histories of the cost functions are shown in Figure 8. The changes of $\mathrm{Real}\,[s_1]$ with respect to the Reynolds number are shown in Figure 9. From this figure, $\mathrm{Re}_\mathrm{C} = 74.8$ and 140.8 at $\mathrm{Re} = 15$ and 40, respectively, and a critical Reynolds number does not exist at $\mathrm{Re} = 30$. The eigenvalue distributions at the initial and optimised shapes, when $\mathrm{Re} = 15$, 30 and 40, are presented in Figure 10.

Based on the results, in the case of the Poiseuille flow field with a sudden expansion, the objective cost functions that decrease monotonically and satisfy the domain measure constraint demonstrate the validity of the approach presented in this paper. Moreover, it can be seen that the first eigenvalues s_1 are always real numbers, and that there exist at least two stable symmetric and asymmetric flow fields (local minimum points) such as those shown in Figure 7 (a) and (b). Among them, the shape shown in Figure 7 (b) is more stable, because a critical Reynolds number is not observed in

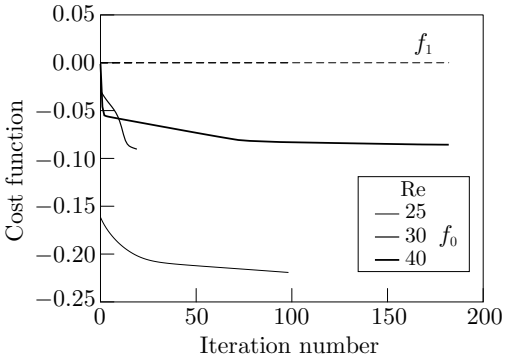

Figure 8. Iteration history of cost functions (Poiseuille flow field).

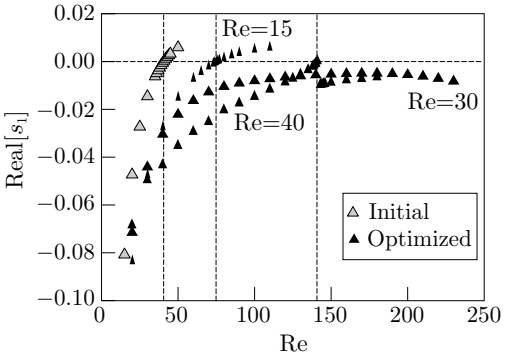

Figure 9. Change of Real$[s_1]$ with respect to the Reynolds number (Poiseuille flow field).

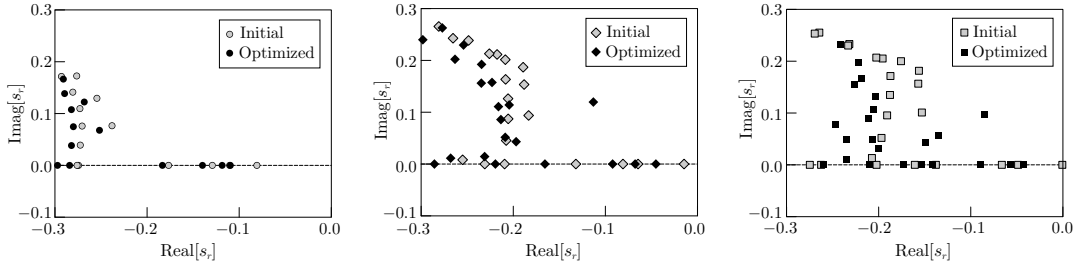

(a) Re = 15 (b) Re = 30 (c) Re = 40

Figure 10. Eigenvalues for initial and optimized shapes at $\boldsymbol{u}_{\mathrm{D}}$ of Re $= 15, 30, 40$ (Poiseuille flow field).

the graph shown in Figure 9.

7.2. *Uniform flow field around isolated body*

Additionally, a two-dimensional uniform flow field around an isolated body was chosen as an example problem because the drag minimisation problem of this flow field has been investigated exclusively as explained in the Introduction. Figure 11 shows the problem setting and initial finite element mesh when $a/b = 1.0$ for Σ_0. The initial domain, Reynolds number and given flow velocity are defined as

$$\Omega_0 = D \setminus \Sigma_0, \quad D = (-10, 25) \times (-10, 10)\,,$$
$$\Sigma_0 = \left\{ (x_1, x_2)^{\mathrm{T}} \in \mathbb{R}^2 \;\middle|\; x_1^2 + x_2^2 < 1 \right\},$$
$$\mathrm{Re}\,(v) = \frac{\rho v \sqrt{|\Sigma\,(\boldsymbol{\phi})|}}{\mu}, \quad \boldsymbol{u}_{\mathrm{D}0} = (v, 0)^{\mathrm{T}} \quad \text{on } \Gamma_{\mathrm{I}0} = \left\{ (0, x_2)^{\mathrm{T}} \in \mathbb{R}^2 \;\middle|\; x_2 \in (-10, 10) \right\}.$$

The original mesh was built into the program by using the following statements:

```
border w1(t=0,1) { x=-10; y=10-20*t; label=inflow;};
border w2(t=0,1) { x=-10+35*t; y=-10; label=slide;};
border w3(t=0,1) { x=25; y=-10+20*t; label=outflow;};
border w4(t=0,1) { x=25-35*t; y=10; label=slide;};
border c(t=0,2*pi) { x=1.0/sqrt(1.0*1.0*pi)*cos(t); y=1.0/sqrt(1.0*1.0*pi)*sin(t); label=wall;};
mesh Th = buildmesh(w1(40)+w2(70)+w3(40)+w4(70)+c(-60));
```

By the adaptive mesh with an error tolerance of err=0.003, the mesh element number in Figure 2 was 12,337. In the domain variation, $\boldsymbol{\phi} = \mathbf{0}_{\mathbb{R}^2}$ on ∂D ($\bar{\Omega}_{\mathrm{C}0} = \partial D$ in (1)) was

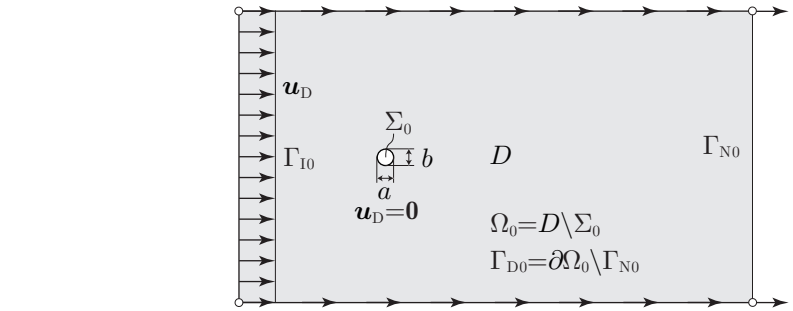

(a) Problem setting

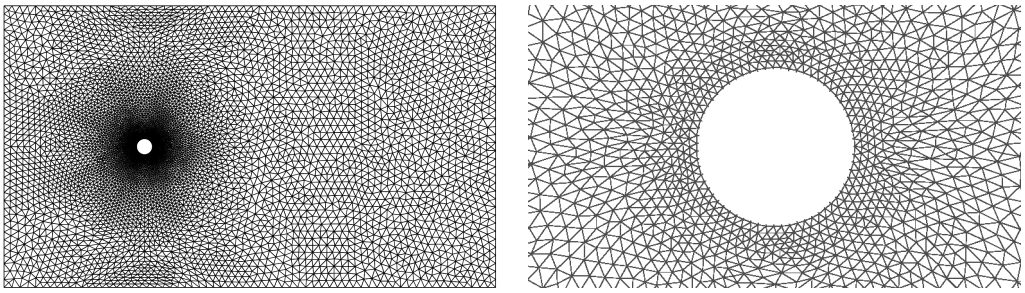

(b) Finite element mesh (c) Zoom of (b)

Figure 11. Uniform flow field around isolated body at initial shape of $a/b = 1.0$.

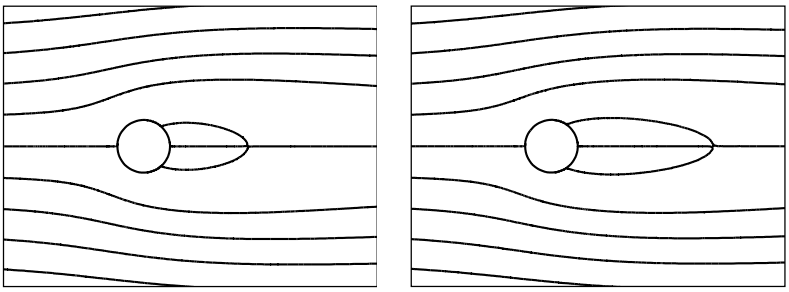

(a) Re = 25 (b) Re = 40

Figure 12. Streamlines at initial shape of $a/b = 1.0$ (isolated body).

assumed. For the step size parameter, $c_a = 5$ was used. In the optimisation process, the number of elements varied from 11,000 to 13,000 by the adaptive mesh.

The streamlines in the stationary Navier–Stokes problem at the initial shape of $a/b = 1.0$ are shown in Figure 12. Figure 13 compares the vortex length results obtained by this study with the results obtained by Acrivos et al. (1968); Taneda (1956); Giannetti and Luchini (2007); Takami and Keller (1969). Moreover, the eigenvalues s_r at the initial shape of $a/b = 1.0$ are illustrated in Figure 14. In this figure, the first three eigenvalues were $s_{1,2} = -0.003921 \pm 0.6965$ i, $s_3 = -0.1092$ (i denotes the imaginary unit) when Re = 40. Figure 15 shows the variation of Real $[s_1]$ with respect to the Reynolds number. From the figure, the critical Reynolds number $\mathrm{Re_C}$ is 40.8. Table 2 compares the values of the $\mathrm{Re_C}$ and critical Strouhal number $\mathrm{St_C}$ ($\mathrm{St} = fl/v$, where l, v and f are the characteristic flow velocity, length and frequency defined by Imag $[s_1]/2\pi$) with the values reported in the literature. This comparison demonstrates the reliability of the analyses conducted by this study. For reference, the first linear disturbance mode (eigenfunction) at Re = 40 is shown in Figure 16.

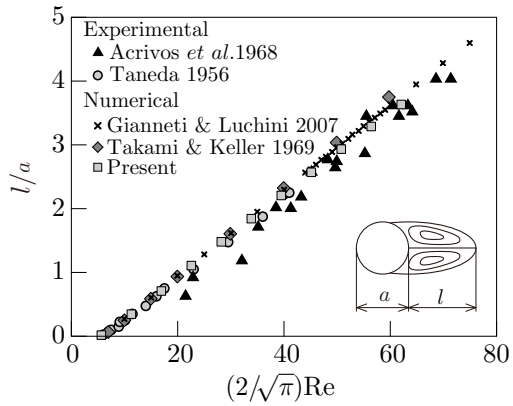

Figure 13. Vortex length at initial shape of $a/b = 1.0$ (isolated body).

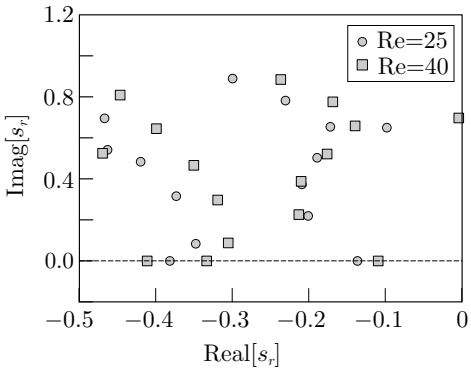

Figure 14. Distribution of eigenvalues s_r at initial shape of $a/b = 1.0$ (isolated body).

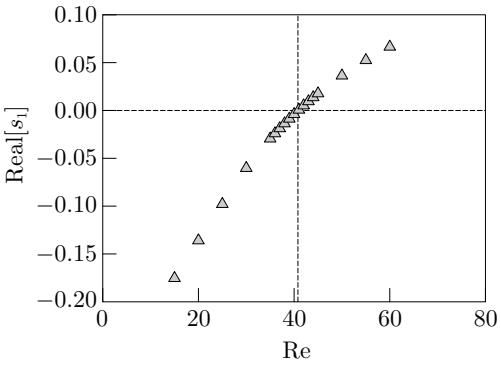

Figure 15. Change of Real $[s_1]$ with respect to Reynolds number at initial shape (isolated body).

The shape optimisation results are shown in Figures 17–20. The shapes and streamlines obtained by using the $\boldsymbol{u}_{\mathrm{D}}$ of Re = 25, 40 and 50 when starting with the initial shapes of representative a/b are shown in Figure 17. In this figure, the shape of (c) was obtained without convergence by turning over the mesh. From the final shapes, it can be considered that a stable shape (local minimum point) may be elliptical, as shown in Figure 17 (a, b, d, f). An elliptical shape with a bluff in the leeward direction, such as that shown in Figure 17 (e), is another possible stable shape.

The iteration histories of the cost functions are shown in Figure 18. In this figure, we notice that the gradients in all graphs of the objective cost function f_0 change when its values approximate -0.3. Figure 19 shows the changes of Real $[s_1]$ with respect to the Reynolds number. From this figure, the critical Reynolds numbers of $\mathrm{Re_C} = 291.1$ and 95.4 at Re = 25 and 40, respectively. The eigenvalue distributions when $a/b = 1.0$

Table 2. Comparison of critical Reynolds and Strouhal numbers when $a/b = 1.0$ (isolated body).

Literature	$2\mathrm{Re_C}$	$2\mathrm{St_C}$
Giannetti and Luchini (2007)	46.7	0.118
Jackson (1987)	45.403	0.13626
Marquet, Sipp, and Jacquin (2008)	46.8	0.116
Chiba (1996)	45.5	0.12
Present study	46.0	0.111

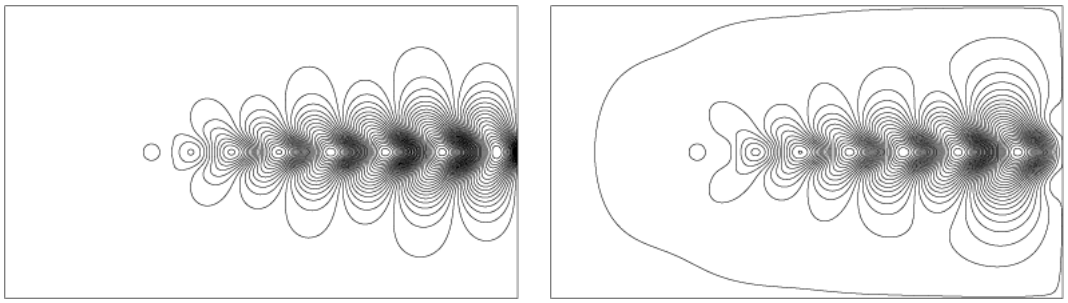

(a) Real part (b) Imaginary part

Figure 16. Linear disturbance mode of first mode at Re = 40 ($a/b = 1.0$).

Table 3. Critical Reynolds numbers $\mathrm{Re_C}$ (isolated body).

a/b	Initial shape	Optimal shape					
		Re = 25	Re = 30	Re = 35	Re = 40	Re = 45	Re = 50
1.0	40.8	291.1	320.0	(140.2)	(95.4)	(99.6)	(88.8)
1.1	44.9	290.9	276.5	307.2	284.6	(142.7)	141.4
1.2	49.2	292.9	296.6	305.9	330.3	349.5	(180.8)
1.3	54.0	292.4	324.8	348.8	329.3	367.6	(142.4)
1.4	59.0	288.0	331.7	364.3	334.7	367.2	311.2
1.5	64.3	291.0	276.3	300.0	333.8	303.1	315.4

$(\cdot)$ denotes no convergence.

are presented in Figure 20, where (a) and (c) show the eigenvalue distributions at the initial and optimised shapes when Re = 25 and 40, respectively, while (b) shows the distributions at the initial and 11th iteration shapes when Re = 25. This distribution illustrates that s_1 had just changed from a complex number to a real number. The 11th iteration in the case of Re = 25 and $a/b = 1.0$ corresponds to the time when f_0 exceeds -0.3. Figure 21 shows the difference in the domain variation at the 10th iteration $\boldsymbol{\varphi}_{g\,10}$ and the difference at the 11th iteration $\boldsymbol{\varphi}_{g\,11}$.

Moreover, we performed additional analyses with more cases. Table 3 symmetrises the results of the critical Reynolds numbers $\mathrm{Re_C}$. In this table, the numbers in parentheses show the values obtained without convergence and corresponding to the elliptical shape with a bluff in the leeward direction, as shown in Figure 17 (b). However, the case of Re = 50 and $a/b = 1.1$ satisfied the convergence condition remarkably.

Based on the results, the validity of the shape optimisation approach, which was presented in this paper, was also verified in the case of a uniform flow field around an isolated body through the monotonic decreasing of the objective cost functions satisfying the domain measure constraint. Moreover, in this case, we confirmed that there existed a stable flow field with an elliptical shape, as shown in Figure 17 (a, b, d, f), and a candidate local minimum point with an elliptical shape and a bluff in the leeward direction was found as shown in Figure 17 (e). By comparing their critical Reynolds numbers, the elliptical shape of Figure 17 (d) was found to be more stable, based on the results presented in Table 3.

8. Conclusion

In this paper, the solution to the shape optimisation problem with regard to the Navier–Stokes flow field proposed by Nakazawa and Azegami (2016) to delay the tran-

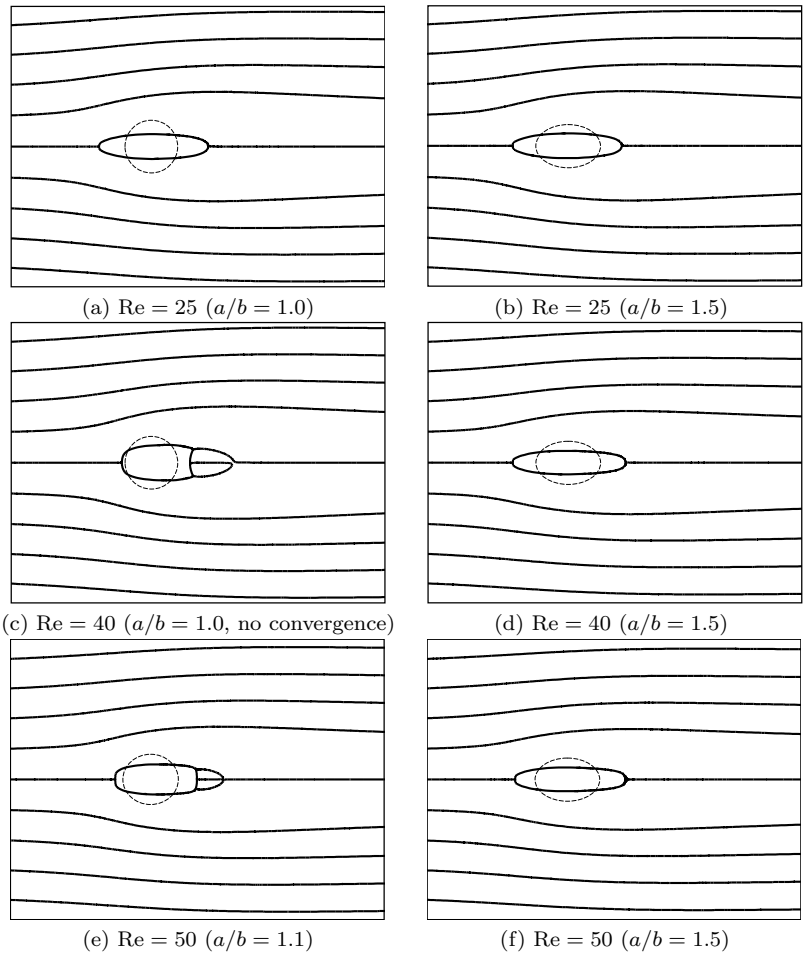

(a) Re = 25 ($a/b = 1.0$) (b) Re = 25 ($a/b = 1.5$)

(c) Re = 40 ($a/b = 1.0$, no convergence) (d) Re = 40 ($a/b = 1.5$)

(e) Re = 50 ($a/b = 1.1$) (f) Re = 50 ($a/b = 1.5$)

Figure 17. Streamlines at optimized shape (isolated body).

sition from laminar to turbulent flow when the velocity increases was reviewed within the framework of functional analysis and updated the theory with another expression of the shape derivative with respect to the objective function. By using a computer program developed with the FreeFEM++ programming language based on theory, numerical analyses with respect to two types of problems, namely, a two-dimensional Poiseuille flow field with a sudden expansion and a two-dimensional uniform flow field around an isolated body, were performed. From the iteration histories of the cost functions, the validity of the proposed approach was verified. Moreover, in the case of the Poiseuille flow field with a sudden expansion, we found that there existed at least two local minimum points of symmetric and asymmetric flow fields, such as those shown in Figure 7 (a) and (b). By comparing the critical Reynolds numbers among them, we confirmed that the asymmetric flow field was more stable. With respect to the two-dimensional uniform flow field around an isolated body, we reached the local minimum point of the elliptical shape, as shown in Figure 17 (a, b, d, f), in almost all cases, and infrequently found a solution converging to an elliptical shape with a bluff in the leeward direction, as shown in Figure 17 (e). By comparing the critical Reynolds numbers of all cases, it became obvious that the elliptical shape shown in Figure 17 (d) was the most stable shape in the numerical results obtained by this study.

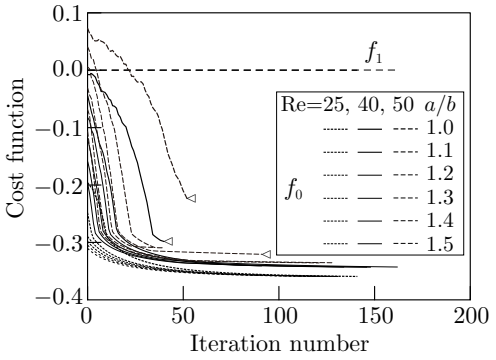

Figure 18. Iteration history of cost functions (isolated body; ◁ denotes no convergence).

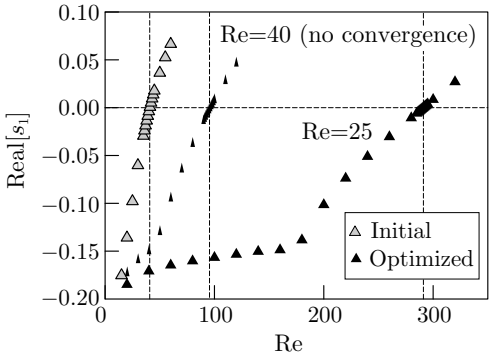

Figure 19. Change of Real $[s_1]$ with respect to Reynolds number (Poiseuille flow field, $a/b = 1.0$).

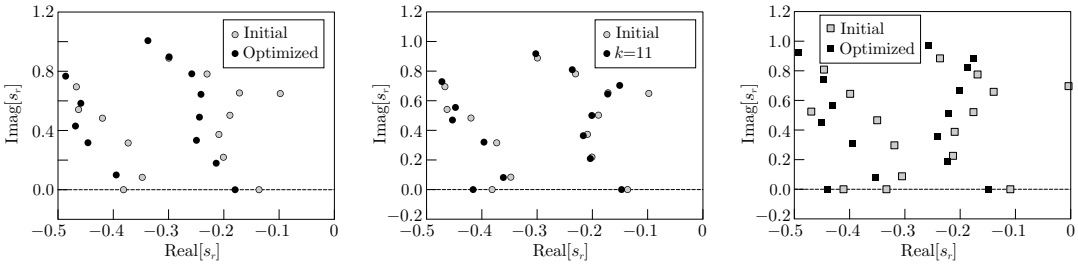

(a) Re = 25 ($a/b = 1.0$) (b) Re = 25 ($a/b = 1.0$) (c) Re = 40 ($a/b = 1.0$)

Figure 20. Eigenvalues for initial and optimized shapes at Re = 25 and 40 (isolated body).

Disclosure statement

No potential conflict of interest was reported by the authors.

Funding

This work was supported by JSPS KAKENHI, Grant Numbers JP16K05285 and JP17K05140.

References

Acrivos, A., L. G. Leal, D. D. Snowden, and F. Pan. 1968. "Further experiments on steady separated flows past bluff objects." *Journal of Fluid Mechanics* 34 (1): 25–48.

Alleborn, N., K. Nandakumar, H. Raszillier, and F. Durst. 1997. "Further contributions on the two-dimensional flow in a sudden expansion." *Journal of Fluid Mechanics* 330: 169–188.

Armijo, L. 1966. "Minimization of functions having Lipschitz-continuous first partial derivatives." *Pacific J. Math.* 16: 1–3.

Azegami, H. 1994. "A Solution to Domain Optimization Problems (in Japanese)." *Transactions of the Japan Society of Mechanical Engineers Series A* 60: 1479–1486.

Azegami, H. 2014. "Regularized Solution to Shape Optimization Problem (in Japanese)." *Transactions of the Japan Society for Industrial and Applied Mathematics* 23 (2): 83–138.

Azegami, H. 2016. *Shape Optimization Problems (in Japanese)*. Tokyo: Morikita Publishing.

Azegami, H., S. Fukumoto, and T. Aoyama. 2013. "Shape Optimization of Continua using

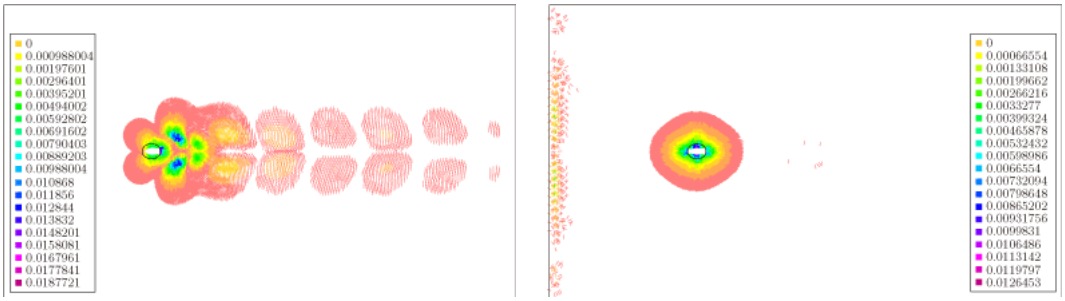

(a) $\varphi_{g\,10}$ (b) $\varphi_{g\,11}$

Figure 21. Domain variations at 10th iteration $\varphi_{g\,10}$ and 11th iteration $\varphi_{g\,11}$ when $\mathrm{Re} = 25$ and $a/b = 1.0$ (isolated body).

NURBS as Basis Functions." *Structural and Multidisciplinary Optimization* 47 (2): 247–258.

Azegami, H., S. Kaizu, and K. Takeuchi. 2011. "Regular Solution to Topology Optimization Problems of Continua." *JSIAM Letters* 3: 1–4.

Azegami, H., and K. Takeuchi. 2006. "A Smoothing Method for Shape Optimization: Traction Method Using the Robin Condition." *International Journal of Computational Methods* 3 (1): 21–33.

Azegami, H., and Z. Q. Wu. 1996. "Domain Optimization Analysis in Linear Elastic Problems: Approach Using Traction Method." *JSME International Journal Series A* 39 (2): 272–278.

Battaglia, F., A. K. Tavener, A. K. Kulkarni, and C. L. Merkle. 1997. "Bifurcation of low Reynolds number flows in symmetric channels." *AIAA Journal* 35: 99–105.

Bello, J. A., E. Fernández-Cara, J. Lemoine, and J. Simon. 1997. "The differentiability of the drag with respect to the variations of a Lipschitz domain in a Navier-Stokes flow." *SIAM Journal on Control and Optimization* 35 (2): 626–640.

Belson, A. B., O. Semeraro, C. W. Rowley, and S. D. Henningson. 2013. "Feedback control of instabilities in the two-dimensional Blasius boundary layer: The role of sensors and actuators." *Physics of Fluids* 25 (054106).

Boujo, E., and F. Gallaire. 2014. "Controlled reattachment in separated flows: a variational approach to recirculation length reduction." *Journal of Fluid Mechanics* 742: 618–635.

Camarri, S., and A. Iollo. 2010. "Feedback control of the vortex-shedding instability based on sensitivity analysis." *Physics of Fluids* 22 (094102).

Chiba, Satoshi. 1996. "Study of global instability of a flow past a circular cylinder." *Journal of Japan Society of Fluid Mechanics* 15 (4): 295–307.

Davis, T. 2004. "Algorithm 832: UMFPACK, an unsymmetric-pattern multifrontal method." *ACM Transactions on Mathematical Software* 30: 196–199.

Fani, A., S. Camarri, and V. M. Salvetti. 2012. "Stability analysis and control of the flow in a symmetric channel with a sudden expansion." *Physics of Fluids* 24 (084102).

Fearn, R. M., T. Mullin, and Cliffe K. A. 1990. "Nonlinear flow phenomena in a symmetric sudden expansion." *Journal of Fluid Mechanics* 211: 595–608.

Ganesh, R.K. 1994. "The minimum drag profile in laminar flow: a numerical way." *Journal of Fluids Engineering* 116: 456–462.

Giannetti, F., and P. Luchini. 2007. "Structural sensitivity of the cylinder wake ' s first instability." *Journal of Fluid Mechanics* 581: 167–197.

Glowinski, R., and O. Pironneau. 1975. "On the numerical computation of minimum-drag profile in laminar flow." *Journal of Fluid Mechanics* 72 (2): 385–389.

Hecht, F. 2012. "New development in FreeFem++." *Journal of Numerical Mathematics* 20 (3-4): 251–265.

Hill, D. C. 1992. "A theoretical approach for analyzing the restabilization of wakes." *AIAA Paper* 1–12. 92-0067.

Huan, J.C., and V. Modi. 1994. "Optimum design of minimum drag bodies in incompressible

laminar flow using a control theory approach." *Inverse Problems in Engineering* 1 (1): 1–25.
Huan, J.C., and V. Modi. 1996. "Design of minimum drag bodies in incompressible laminar flow." *Inverse Problems in Engineering* 3 (1): 233–260.
Ishiyama, H., and M. Kawahara. 2008. "Shape optimization of body located in incompressible viscous flow." *International Journal of Computer Mathematics* 85 (10): 1515–1530.
Jackson, C. P. 1987. "A finite-element study of the onset of vortex shedding in flow past variously shaped bodies." *Journal of Fluid Mechanics* 182: 23–45.
Jameson, A. 1988. "Aerodynamic design via control theory." *Journal of Scientific Computing* 3 (3): 233–260.
Jameson, A. 1995. *Computational Fluid Dynamics Review 1995*, Chap. Optimum aerodynamic design using control theory, 495–528. New York: Wiley.
Katamine, E., H. Azegami, T. Tsubata, and S. Itoh. 2005. "Solution to Shape Optimization Problems of Viscous Flow Fields." *International Journal of Computational Fluid Dynamics* 19 (1): 45–51.
Katamine, E., Y. Nagatomo, and H. Azegami. 2009. "Shape Optimization of 3D Viscous Flow Fields." *Inverse Problems in Science and Engineering* 17 (1): 105–114.
Marquet, O., D. Sipp, and L. Jacquin. 2008. "Sensitivity analysis and passive control of cylinder flow." *J. Fluid. Mech.* 615: 221–252.
Mittal, S., and A. Raghuvanshi. 2001. "Control of vortex shedding behind circular cylinder for flows at low Reynolds number." *International Journal for Numerical Methods in Fluids* 37: 421–447.
Mizushima, J., and Y. Shiotani. 2000. "Structural instability of the bifurcation diagram for two-dimensional flow in a channel with a sudden expansion." *Journal of Fluid Mechanics* 420: 131–145.
Mohammadi, B. 1997. "A new optimal shape design procedure for inviscid and viscous turbulent flows." *International Journal for Numerical Methods in Fluids* 25: 183–203.
Mohammadi, B., and O. Pironneau. 2001. *Applied shape optimization for fluids*. Oxford, New York: Oxford University Press.
Nakazawa, T., and H. Azegami. 2016. "Shape Optimization of Flow Field Improving Hydrodynamic Stability." *Japan Journal of Industrial and Applied Mathematics* 33 (1): 167–181.
Ogawa, Y., and M. Kawahara. 2003. "Shape optimization of body located in incompressible viscous flow based on optimal control theory." *International Journal of Computational Fluid Dynamics* 17: 243–251.
Pironneau, O. 1973. "On optimum profiles in Stokes flow." *Journal of Fluid Mechanics* 59 (1): 117–128.
Pironneau, O. 1974. "On Optimum Design in Fluid Mechanics." *Journal of Fluid Mechanics* 64 (1): 97–110.
Pironneau, O. 1984. *Optimal Shape Design for Elliptic Systems*. New York: Springer-Verlag.
Sakamoto, M., and M. Kawahara. 2011. "Shape optimization of a body located in incompressible flow using adjoint method and partial control algorithm." *International Journal for Numerical Methods in Fluids* 67: 1702–1719.
Sano, M., and H. Sakai. 1982. "Numerical determination of minimum drag profile in Stokes flow (in case of two-dimensional finite region and constant cross-sectional area)." *Journal of the Japan Society for Aeronautical and Space Sciences* 30 (339): 207–213.
Sipp, D., O. Marquet, P. Meliga, and A. Barbagallo. 2010. "Dynamics and control of global instabilities in open flows: a linearized approach." *Applied Mechanics Reviews* 63 (030801): 1–26.
Strykowski, P. J., and K. R. Sreenivasan. 1990. "On the formation and suppression of vortex 'shedding' at low Reynolds numbers." *Journal of Fluid Mechanics* 218: 71–107.
Takami, H., and H. B. Keller. 1969. "Steady two-dimensional viscous flow of an incompressible fluid past a circular cylinder." *The Physics of Fluids* 12 (12): II51–II56.
Taneda, S. 1956. "Experimental investigation of the wakes behind cylinders and plates at low Reynolds numbers." *Journal of the Physical Society of Japan* 11 (3): 302–307.
Yagi, H., and M. Kawahara. 2005. "Shape optimization of a body located in low Reynolds

number." *International Journal for Numerical Methods in Fluids* 48: 819–833.
Yagi, H., and M. Kawahara. 2007. "Optimal shape determination of a body located in incompressible viscous fluid flows." *Computer Methods in Applied Mechanics and Engineering* 196: 5084–5091.
Zebib, A. 1987. "Stability of viscous flow past a circular cylinder." *Journal of Engineering Mathematics* 21: 155–165. 92-0067.

Appendices

Appendix 1. *Definitions of shape derivatives*

In a problem where the domain moves, the functions and integrals defined in the problem vary with the variation of the domain. Here, we define their Fréchet derivatives.

Let $\boldsymbol{\phi} \in \mathcal{D}$ be given, and $\boldsymbol{\varphi} \in \mathcal{D}$ be an arbitrary domain variation from $\Omega(\boldsymbol{\phi})$. When the domain moves from $\Omega(\boldsymbol{\phi})$ to $\Omega(\boldsymbol{\phi}+\boldsymbol{\varphi})$, the function defined in it is also assumed to change. In this case, when $\boldsymbol{\phi}$, we can write the function as $u(\boldsymbol{\phi})$, and the value at point $\boldsymbol{x}$ in the expanded domain $\mathbb{R}^d$ of $\Omega(\boldsymbol{\phi})$ as $u(\boldsymbol{\phi})(\boldsymbol{x})$. This notation can be used to define the shape derivative of the function as described later.

Definition A.1 (Shape derivative of function)**.** *Let us suppose that the functions $u : \mathcal{D} \to L^2\left(\mathbb{R}^d;\mathbb{R}\right)$ and $\boldsymbol{\phi} \in \mathcal{D}$ are given. If there exists a bounded linear operator $u'(\boldsymbol{\phi})[\,\cdot\,] : \mathcal{D} \to L^2\left(\mathbb{R}^d;\mathbb{R}\right)$ satisfying*

$$u(\boldsymbol{\phi}+\boldsymbol{\varphi})(\boldsymbol{x}+\boldsymbol{\varphi}(\boldsymbol{x})) = u(\boldsymbol{\phi})(\boldsymbol{x}) + u'(\boldsymbol{\phi})[\boldsymbol{\varphi}](\boldsymbol{x}) + o\left(\|\boldsymbol{\varphi}(\boldsymbol{x})\|_X\right) \quad \forall \boldsymbol{\varphi} \in \mathcal{D}$$

almost everywhere in $\boldsymbol{x} \in \mathbb{R}^d$, and $u'(\boldsymbol{\phi})[\,\cdot\,] : X \to L^2\left(\mathbb{R}^d;\mathbb{R}\right)$ is also a bounded linear operator, then, $u'(\boldsymbol{\phi})[\boldsymbol{\varphi}]$ is referred to as the shape derivative at $\boldsymbol{\phi} \in \mathcal{D}$ of u and can be written as $u \in C^1\left(\mathcal{D}; L^2\left(\mathbb{R}^d;\mathbb{R}\right)\right)$.

In continuum mechanics, $u(\boldsymbol{\phi}+\boldsymbol{\varphi})(\boldsymbol{x}+\boldsymbol{\varphi}(\boldsymbol{x}))$ in Definition .1 is called the Lagrangian description of $u(\boldsymbol{\phi})(\boldsymbol{x})$, and $u'(\boldsymbol{\phi})[\boldsymbol{\varphi}]$ is called the material derivative.

The shape derivative of a functional defined on a moving domain is defined as follows. Here, we use the notation of $\boldsymbol{\nabla}_z = \left(\partial(\,\cdot\,)/z_1, \ldots, \partial(\,\cdot\,)/z_d\right)^{\mathrm{T}}$ with respect to $\boldsymbol{z} \in \Omega(\boldsymbol{\phi}+\boldsymbol{\varphi})$. Moreover, let $\boldsymbol{\nu}(\boldsymbol{\phi})$ be the outward unit normal defined at boundary $\partial\Omega(\boldsymbol{\phi})$, $\partial_\nu(\,\cdot\,) = \boldsymbol{\nu}(\boldsymbol{\phi}) \cdot \boldsymbol{\nabla}(\,\cdot\,)$, $\boldsymbol{\mu} = \boldsymbol{\nu}(\boldsymbol{\phi}+\boldsymbol{\varphi})$ be the outward unit normal on $\partial\Omega(\boldsymbol{\phi}+\boldsymbol{\varphi})$, and $\partial_\mu(\,\cdot\,) = \boldsymbol{\mu} \cdot \boldsymbol{\nabla}_z$. Moreover, the dual space of X is denoted as X'.

Definition A.2 (Shape derivative of functional)**.** *Suppose*

$$h_0 \in C^1\left(C^1\left(\mathcal{D}; H^1\left(\mathbb{R}^d;\mathbb{R}\right)\right) \times C^1\left(\mathcal{D}; L^2\left(\mathbb{R}^d;\mathbb{R}^d\right)\right); L^2\left(\mathbb{R}^d;\mathbb{R}\right)\right),$$
$$h_1 \in C^1\left(C^1\left(\mathcal{D}; H^2\left(\mathbb{R}^d;\mathbb{R}\right)\right) \times C^1\left(\mathcal{D}; H^1\left(\mathbb{R}^d;\mathbb{R}\right)\right); H^1\left(\mathbb{R}^d;\mathbb{R}\right)\right)$$

and $\boldsymbol{\phi} \in \mathcal{D}$ are given. Let

$$f\left(\boldsymbol{\phi}+\boldsymbol{\varphi}, u(\boldsymbol{\phi}+\boldsymbol{\varphi}), \boldsymbol{\nabla}_z u(\boldsymbol{\phi}+\boldsymbol{\varphi}), \partial_\mu u(\boldsymbol{\phi}+\boldsymbol{\varphi})\right)$$
$$= \int_{\Omega(\boldsymbol{\phi}+\boldsymbol{\varphi})} h_0\left(u(\boldsymbol{\phi}+\boldsymbol{\varphi})(\boldsymbol{z}), \boldsymbol{\nabla}_z u(\boldsymbol{\phi}+\boldsymbol{\varphi})(\boldsymbol{z})\right) \mathrm{d}z$$

$$+\int_{\Gamma(\boldsymbol{\phi}+\boldsymbol{\varphi})} h_1\left(u\left(\boldsymbol{\phi}+\boldsymbol{\varphi}\right)(\boldsymbol{z}), \partial_\mu u\left(\boldsymbol{\phi}+\boldsymbol{\varphi}\right)(\boldsymbol{z})\right) \mathrm{d}\zeta \quad \forall \boldsymbol{\varphi} \in \mathcal{D}. \tag{A1}$$

Here, $\Gamma(\boldsymbol{\phi})$ *is considered as the partial set of* $\partial\Omega(\boldsymbol{\phi})$ *(allowing* $\Gamma(\boldsymbol{\phi}) = \partial\Omega(\boldsymbol{\phi})$*). Moreover,* $\mathrm{d}z$ *and* $\mathrm{d}\zeta$ *represent the infinitesimal measures used in the domain and boundary integrals when* $\Omega(\boldsymbol{\phi}+\boldsymbol{\varphi})$*. In this case, if a bounded and linear functional* $f'\left(\boldsymbol{\phi}, u(\boldsymbol{\phi}), \boldsymbol{\nabla} u(\boldsymbol{\phi}), \partial_\nu u(\boldsymbol{\phi})\right)[\cdot] : \mathcal{D} \to \mathbb{R}$ *satisfies*

$$\begin{aligned} &f\left(\boldsymbol{\phi}+\boldsymbol{\varphi}, u\left(\boldsymbol{\phi}+\boldsymbol{\varphi}\right), \boldsymbol{\nabla}_z u\left(\boldsymbol{\phi}+\boldsymbol{\varphi}\right), \partial_\mu u\left(\boldsymbol{\phi}+\boldsymbol{\varphi}\right)\right) \\ &\quad = f\left(\boldsymbol{\phi}, u(\boldsymbol{\phi}), \boldsymbol{\nabla} u(\boldsymbol{\phi}), \partial_\nu(\boldsymbol{\phi})\right) \\ &\qquad + f'\left(\boldsymbol{\phi}, u(\boldsymbol{\phi}), \boldsymbol{\nabla} u(\boldsymbol{\phi}), \partial_\nu(\boldsymbol{\phi})\right)[\boldsymbol{\varphi}] + o\left(\|\boldsymbol{\varphi}\|_X\right) \end{aligned}$$

and $f'\left(\boldsymbol{\phi}, u(\boldsymbol{\phi}), \boldsymbol{\nabla} u(\boldsymbol{\phi}), \partial_\nu u(\boldsymbol{\phi})\right)[\cdot] : X \to \mathbb{R}$ *is also a bounded and linear functional. In other words, if there exists* $\boldsymbol{g} \in X'$ *such that* $f'\left(\boldsymbol{\phi}, u(\boldsymbol{\phi}), \boldsymbol{\nabla} u(\boldsymbol{\phi}), \partial_\nu u(\boldsymbol{\phi})\right)[\boldsymbol{\varphi}] = \langle \boldsymbol{g}, \boldsymbol{\varphi} \rangle$ *can be written,* f *is said to be shape derivable, and* $\boldsymbol{g}$ *is called the shape gradient of* f*. In this case,* $f \in C^1(\mathcal{D}; \mathbb{R})$*.*

Appendix 2. *Shape derivatives of functionals*

In Section 5.1, the following results were used.

Proposition A.3 (Shape derivative of domain integral (Azegami 2016, Proposition 9.3.4))**.** $\boldsymbol{\phi}$*,* u *and* $\boldsymbol{\nabla} u$ *are elements of* $\mathcal{D}$*,* $\mathcal{U} = C^1\left(\mathcal{D}, H^1\left(\mathbb{R}^d, \mathbb{R}\right)\right)$ *and* $\mathcal{V} = C^1\left(\mathcal{D}, L^2\left(\mathbb{R}^d, and \mathbb{R}^d\right)\right)$*, respectively.* $h(u, \boldsymbol{\nabla} u)$ *was considered as an element of* $C^1\left(\mathcal{U} \times \mathcal{V}; L^2\left(\mathbb{R}^d; \mathbb{R}\right)\right)$*. Let*

$$f\left(\boldsymbol{\phi}+\boldsymbol{\varphi}, u\left(\boldsymbol{\phi}+\boldsymbol{\varphi}\right), \boldsymbol{\nabla}_z u\left(\boldsymbol{\phi}+\boldsymbol{\varphi}\right)\right) = \int_{\Omega(\boldsymbol{\phi}+\boldsymbol{\varphi})} h\left(u\left(\boldsymbol{\phi}+\boldsymbol{\varphi}\right), \boldsymbol{\nabla}_z u\left(\boldsymbol{\phi}+\boldsymbol{\varphi}\right)\right) \mathrm{d}z.$$

In this case, the shape derivative of f *becomes*

$$\begin{aligned} &f'(\boldsymbol{\phi}, u, \boldsymbol{\nabla} u)[\boldsymbol{\varphi}] \\ &\quad = \int_{\Omega(\boldsymbol{\phi})} \left\{ h_u(u, \boldsymbol{\nabla} u)\left[u'\right] + h_{\boldsymbol{\nabla} u}(u, \boldsymbol{\nabla} u)\left[\boldsymbol{\nabla} u' - \left(\boldsymbol{\nabla} \boldsymbol{\varphi}^{\mathrm{T}}\right) \boldsymbol{\nabla} u\right] + h(u, \boldsymbol{\nabla} u)\, \boldsymbol{\nabla} \cdot \boldsymbol{\varphi} \right\} \mathrm{d}x \\ &\qquad \forall \boldsymbol{\varphi} \in X. \end{aligned} \tag{A2}$$

Based on the result in Proposition .3, $f(\boldsymbol{\phi}, u, \boldsymbol{\nabla} u)$ can be written as $f(\boldsymbol{\phi}, u)$, and (2) can be written as

$$f'(\boldsymbol{\phi}, u, \boldsymbol{\nabla} u)[\boldsymbol{\varphi}] = f'(\boldsymbol{\phi}, u)\left[\boldsymbol{\varphi}, u'\right] = f_{\boldsymbol{\phi}}(\boldsymbol{\phi}, u)[\boldsymbol{\varphi}] + f_u(\boldsymbol{\phi}, u)\left[u'\right] \tag{A3}$$

in Section 5.1. Here,

$$\begin{aligned} f_{\boldsymbol{\phi}}(\boldsymbol{\phi}, u)[\boldsymbol{\varphi}] &= \int_{\Omega(\boldsymbol{\phi})} \left\{ h_{\boldsymbol{\nabla} u}(u, \boldsymbol{\nabla} u)\left[-\left(\boldsymbol{\nabla} \boldsymbol{\varphi}^{\mathrm{T}}\right) \boldsymbol{\nabla} u\right] + h(u, \boldsymbol{\nabla} u)\, \boldsymbol{\nabla} \cdot \boldsymbol{\varphi} \right\} \mathrm{d}x, \\ f_u(\boldsymbol{\phi}, u)\left[u'\right] &= \int_{\Omega(\boldsymbol{\phi})} \left\{ h_u(u, \boldsymbol{\nabla} u)\left[u'\right] + h_{\boldsymbol{\nabla} u}(u, \boldsymbol{\nabla} u)\left[\boldsymbol{\nabla} u'\right] \right\} \mathrm{d}x. \end{aligned}$$

When the integrand of a boundary integral is given by the function of u and $\partial_\nu u$, the following results can be obtained. Here, the tangent on $\partial\Omega(\boldsymbol{\phi})$ can be written as $\boldsymbol{\tau}_1(\boldsymbol{\phi}), \ldots, \boldsymbol{\tau}_{d-1}(\boldsymbol{\phi})$. Moreover, $\boldsymbol{\nabla}_\tau(\cdot) = (\boldsymbol{\tau}_j(\boldsymbol{\phi}) \cdot \boldsymbol{\nabla})_{j\in\{1,\ldots,d-1\}}(\cdot) \in \mathbb{R}^{d-1}$, $\boldsymbol{\varphi}_\tau = (\boldsymbol{\tau}_j(\boldsymbol{\phi}) \cdot \boldsymbol{\varphi})_{j\in\{1,\ldots,d-1\}} \in \mathbb{R}^{d-1}$ and $(\boldsymbol{\nabla}\cdot\boldsymbol{\varphi})_\tau = \boldsymbol{\nabla}\cdot\boldsymbol{\varphi} - \boldsymbol{\nu}(\boldsymbol{\phi}) \cdot \left(\boldsymbol{\nabla}\boldsymbol{\varphi}^{\mathrm{T}}\boldsymbol{\nu}(\boldsymbol{\phi})\right)$. For simplicity, $\boldsymbol{\nu}(\boldsymbol{\phi})$ and $\boldsymbol{\tau}_1(\boldsymbol{\phi}), \ldots, \boldsymbol{\tau}_{d-1}(\boldsymbol{\phi})$ can be written as $\boldsymbol{\nu}$ and $\boldsymbol{\tau}_1, \ldots, \boldsymbol{\tau}_{d-1}$. Additionally, for the set of corner points (when $d = 2$) or edges (when $d = 3$) in the $\partial\Omega(\boldsymbol{\phi})$, we use the notation of $\Theta(\boldsymbol{\phi})$.

Proposition A.4 (Shape derivative of boundary integral (Azegami 2016, Proposition 9.3.7))**.** *$\boldsymbol{\phi}$, u and $\partial_\nu u$ are elements of $\mathcal{D}$, $\mathcal{U} = C^1\left(\mathcal{D}, H^2\left(\mathbb{R}^d, \mathbb{R}\right)\right)$ and $\mathcal{V} = C^1\left(\mathcal{D}, H^1\left(\mathbb{R}^d, and\mathbb{R}\right)\right)$, respectively. $h(u, \partial_\nu u)$ is an element of $C^1\left(\mathcal{U}\times\mathcal{V}, H^1\left(\mathbb{R}, and\mathbb{R}\right)\right)$. Let*

$$
\begin{aligned}
&f\left(\boldsymbol{\phi}+\boldsymbol{\varphi}, u\left(\boldsymbol{\phi}+\boldsymbol{\varphi}\right), \partial_\mu u\left(\boldsymbol{\phi}+\boldsymbol{\varphi}\right)\right)\\
&\quad = \int_{\Gamma(\boldsymbol{\phi}+\boldsymbol{\varphi})} h\left(u\left(\boldsymbol{\phi}+\boldsymbol{\varphi}\right), \partial_\mu u\left(\boldsymbol{\phi}+\boldsymbol{\varphi}\right)\right) \mathrm{d}\zeta \quad \forall\boldsymbol{\varphi} \in \mathcal{D}.
\end{aligned}
$$

In this case, the shape derivative of f becomes

$$
\begin{aligned}
&f'\left(\boldsymbol{\phi}, u, \partial_\nu u\right)[\boldsymbol{\varphi}]\\
&\quad = \int_{\Gamma(\boldsymbol{\phi})} \Big\{ h_u\left(u, \partial_\nu u\right)\left[u'\right] + h_{\partial_\nu u}\left(u, \partial_\nu u\right)\left[\partial_\nu u' + w\left(\boldsymbol{\varphi}, u\right)\right]\\
&\qquad + h\left(u, \partial_\nu u\right)\left(\boldsymbol{\nabla}\cdot\boldsymbol{\varphi}\right)_\tau \Big\} \mathrm{d}\gamma \quad \forall\boldsymbol{\varphi} \in H^2\left(\mathbb{R}^d; \mathbb{R}^d\right),
\end{aligned}
$$

where

$$
w\left(\boldsymbol{\varphi}, u\right) = \left[\left\{\boldsymbol{\nu}\cdot\left(\boldsymbol{\nabla}\boldsymbol{\varphi}^{\mathrm{T}}\boldsymbol{\nu}\right)\right\}\boldsymbol{\nu} - \left\{\left(\boldsymbol{\nabla}\boldsymbol{\varphi}^{\mathrm{T}} + \left(\boldsymbol{\nabla}\boldsymbol{\varphi}^{\mathrm{T}}\right)^{\mathrm{T}}\right\}\boldsymbol{\nu}\right] \cdot \boldsymbol{\nabla} u.
$$

Moreover, if $\Gamma(\boldsymbol{\phi})$ is a piecewise C^2 class, then,

$$
\begin{aligned}
&f'\left(\boldsymbol{\phi}, u, \partial_\nu u\right)[\boldsymbol{\varphi}]\\
&\quad = \int_{\Gamma(\boldsymbol{\phi})} \Big\{ h_u\left(u, \partial_\nu u\right)\left[u'\right] + h_{\partial_\nu u}\left(u, \partial_\nu u\right)\left[\partial_\nu u' + w\left(\boldsymbol{\varphi}, u\right)\right]\\
&\qquad + \kappa h\left(u, \partial_\nu u\right)\boldsymbol{\nu}\cdot\boldsymbol{\varphi} - \boldsymbol{\nabla}_\tau h\left(u, \partial_\nu u\right)\cdot\boldsymbol{\varphi}_\tau \Big\} \mathrm{d}\gamma\\
&\qquad + \int_{\partial\Gamma(\boldsymbol{\phi})\cup\Theta(\boldsymbol{\phi})} h\left(u, \partial_\nu u\right)\boldsymbol{\tau}\cdot\boldsymbol{\varphi}\, \mathrm{d}\varsigma
\end{aligned} \tag{A4}
$$

is obtained, where $\kappa = \boldsymbol{\nabla}\cdot\boldsymbol{\nu}$.

From the result in Proposition .4, we can write $f\left(\boldsymbol{\phi}, u, \partial_\nu u\right)$ as $f\left(\boldsymbol{\phi}, u\right)$, and (4) as

$$
f'\left(\boldsymbol{\phi}, u\right)\left[\boldsymbol{\varphi}, u'\right] = f_{\boldsymbol{\phi}}\left(\boldsymbol{\phi}, u\right)[\boldsymbol{\varphi}] + f_u\left(\boldsymbol{\phi}, u\right)\left[u'\right], \tag{A5}
$$

where

$$
f_{\boldsymbol{\phi}}\left(\boldsymbol{\phi}, u\right)[\boldsymbol{\varphi}] = \int_{\Gamma(\boldsymbol{\phi})} \left\{h_{\partial_\nu u}\left(u, \partial_\nu u\right)\left[w\left(\boldsymbol{\varphi}, u\right)\right] + h\left(u, \partial_\nu u\right)\left(\boldsymbol{\nabla}\cdot\boldsymbol{\varphi}\right)_\tau\right\} \mathrm{d}\gamma,
$$

$$f_u(\boldsymbol{\phi}, u)\left[u'\right] = \int_{\Gamma(\boldsymbol{\phi})} \left(h_u(u, \partial_\nu u)\left[u'\right] + h_{\partial_\nu u}(u, \partial_\nu u)\left[\partial_\nu u'\right]\right) \mathrm{d}\gamma.$$

Furthermore, if $\Gamma(\boldsymbol{\phi})$ is a piecewise C^2 class, then,

$$\begin{aligned} & f_{\boldsymbol{\phi}}(\boldsymbol{\phi}, u)[\boldsymbol{\varphi}] \\ & = \int_{\Gamma(\boldsymbol{\phi})} \Big(h_{\partial_\nu u}(u, \partial_\nu u)\left[w(\boldsymbol{\varphi}, u)\right] + \kappa h(u, \partial_\nu u)\,\boldsymbol{\nu}\cdot\boldsymbol{\varphi} - \boldsymbol{\nabla}_\tau h(u, \partial_\nu u)\cdot\boldsymbol{\varphi}_\tau\Big)\mathrm{d}\gamma \\ & \quad + \int_{\partial\Gamma(\boldsymbol{\phi})\cup\Theta(\boldsymbol{\phi})} h(u, \partial_\nu u)\,\boldsymbol{\tau}\cdot\boldsymbol{\varphi}\,\mathrm{d}\varsigma. \end{aligned}$$